

國立交通大學

電信工程學系碩士班 碩士論文

直接序列超寬頻系統於密集路徑通道下之
同步與等化技術之研究



Synchronization and Equalization for DS-UWB
System over Dense Multipath Channel

研究生：鄭永立

Student: Yung-Li Cheng

指導教授：李大嵩 博士

Advisor: Dr. Ta-Sung Lee

中華民國九十四年六月

國立交通大學

電信工程學系碩士班 碩士論文

直接序列超寬頻系統於密集路徑通道下之
同步與等化技術之研究



Synchronization and Equalization for DS-UWB
System over Dense Multipath Channel

研究生：鄭永立

Student: Yung-Li Cheng

指導教授：李大嵩 博士

Advisor: Dr. Ta-Sung Lee

中華民國九十四年六月

直接序列超寬頻系統於密集路徑通道下之
同步與等化技術之研究

Synchronization and Equalization for DS-UWB
System over Dense Multipath Channel

研 究 生：鄭永立

Student: Yung-Li Cheng

指 導 教 授：李大嵩 博士

Advisor: Dr. Ta-Sung Lee



A Thesis

Submitted to Department of Communication Engineering
College of Electrical Engineering and Computer Science

National Chiao Tung University

in Partial Fulfillment of the Requirements

for the Degree of

Master of Science

in

Communication Engineering

June 2005

Hsinchu, Taiwan, Republic of China

中華民國九十四年六月

直接序列超寬頻系統於密集路徑通道下之 同步與等化技術之研究

學生：鄭永立

指導教授：李大嵩 博士

國立交通大學電信工程學系碩士班

摘要

超寬頻技術近年來於高速室內無線通訊受到極大的矚目，此乃因為超寬頻系統的傳輸資料率在數公尺的距離下能達到數百 Mbps。在這類技術當中，使用直接序列展頻是最被廣泛熟知的技術來符合超寬頻信號的規定。在本論文中，吾人提出一種具有增強型先-遲碼追蹤迴路(early-late code tracking loop)與選擇性前置犁耙分集結合(S-Pre-Rake diversity combining)能力之 IEEE 802.15.3a 直接序列超寬頻(DS-UWB)系統。由於超寬頻系統所傳送的極短脈衝可解析出許多的路徑，因此通道響應將會由密集的多路徑所組成，並具有長延遲擴散(long delay spread)的特性。傳統的先-遲碼追蹤迴路的效能會因為緊密間隔的多路徑符元間干擾而大幅下降，為了克服此一問題，吾人可採用增強型先-遲碼追蹤迴路有效地消除干擾。另一方面，接收信號能量會散佈於長延遲擴散的多路徑上並造成嚴重的符元間干擾，雖然使用一長階數等化器可有效地還原通道所造成之效應，但其複雜度卻會太高。吾人所提出之傳送端選擇性前置犁耙分集結合器與接收端簡化等化器於之共同設計可大幅降低等化器複雜度並同時達成分集結合和符元間干擾消除之目的。最後，吾人藉由電腦模擬驗證上述架構在室內超寬頻環境中，具有可靠的傳輸效能。

Synchronization and Equalization for DS-UWB System over Dense Multipath Channel

Student: Yung-Li Cheng

Advisor: Dr. Ta-Sung Lee

Department of Communication Engineering

National Chiao Tung University

Abstract

Ultrawideband (UWB) technologies have attracted much attention in high speed indoor wireless communications recently since the transmission data rate of UWB can achieve hundreds of megabits per second over distances of several meters. Among them, direct sequence spread spectrum (DSSS) is the most well-known approach to meeting regulations of UWB signal. In this thesis, an IEEE 802.15.3a DS-UWB system with enhanced early-late (EL) code tracking loop and selective-Pre-Rake (S-Pre-Rake) diversity combining schemes is proposed. UWB system can resolve many paths due to the ultra short transmitted pulses; hence the channel response will be composed of dense multipaths and have a long delay spread. The performance of conventional EL code-tracking loop is typically significantly degraded due to the closely spaced multipath intersymbol interference (ISI). To mitigate this problem, the enhanced EL code tracking scheme is adopted to effectively remove the interference. On the other hand, the received energy is distributed over long delay spread multipaths which will induce serious ISI effect. Although an equalizer with a large number taps can restore the channel effect, its complexity may be probability high. The proposed joint design of S-Pre-Rake combiner at the transmitter and simplified equalizer at the receiver can greatly alleviate the equalizer complexity and achieve both diversity combining and ISI elimination simultaneously. We evaluate the performance of the proposed system and confirm that it works reliably in indoor UWB environments.

Acknowledgement

I would like to express my deepest gratitude to my advisor, Dr. Ta-Sung Lee, for his enthusiastic guidance and great patience. Heartfelt thanks are also offered to all members in the Communication Signal Processing (CSP) Lab for their constant encouragement. Last but not least, I would like to show my sincere appreciation and love to my family for their life-long love and support.



Contents

Chinese Abstract	I
English Abstract	II
Acknowledgement	III
Contents	IV
List of Figures	VI
List of Tables	IX
Acronym Glossary	X
Notations	XIII
1 Introduction	1
2 Overview of IEEE 802.15.3a DS-UWB System	4
2.1 Review of Spread Spectrum System.....	5
2.1.1 Direct Sequence Spread Spectrum.....	5
2.2 IEEE 802.15.3a DS-UWB System	7
2.2.1 Modulation for Data, Header and Preamble	9
2.2.2 PHY Preamble and Header Components.....	10
2.2.3 Transmitter Architecture	11
2.2.4 Multiple Access Scheme.....	14
2.3 Summary.....	16



3	Performance of IEEE 802.15.3a DS-UWB System	28
3.1	Indoor UWB Channel Model.....	28
3.1.1	Saleh-Valenzuela Model.....	29
3.2	Synchronization Techniques for IEEE 802.15.3a DS-UWB System.....	33
3.2.1	Code Acquisition.....	34
3.2.2	Code-Tracking Loop.....	34
3.2.3	Automatic Frequency Control Loop.....	37
3.3	Channel Equalization for IEEE 802.15.3a DS-UWB System.....	38
3.4	Computer Simulations.....	40
3.5	Summary.....	41
4	Pre-Rake Diversity Combining Technique for IEEE 802.15.3a DS-UWB System	59
4.1	Pre-Rake Diversity Combining for DSSS Communications Systems.....	60
4.1.1	Diversity Combining Methods.....	60
4.1.2	Rake Combining Scheme.....	61
4.1.3	Pre-Rake Combining Scheme.....	62
4.2	Pre-Rake Diversity Combining for IEEE 802.15.3a DS-UWB System.....	62
4.3	Channel Estimation for IEEE 802.15.3a DS-UWB System.....	64
4.3.1	Channel Estimation via Correlation.....	65
4.3.2	Channel Estimation with Sidelobe Cancellation.....	66
4.4	Simplified Receiver Architecture.....	67
4.4.1	Post-Cursor Multipath Cancellation.....	67
4.5	Computer Simulations.....	68
4.6	Summary.....	69
5	Conclusion	81
	Bibliography	85

List of Figures

Figure 2.1	UWB spectral mask for indoor communication system	17
Figure 2.2	Model of spread spectrum digital communication system	17
Figure 2.3	PN and data signal	18
Figure 2.4	Block diagram of a DSSS communication system	18
Figure 2.5	Spectrum mask of IEEE 802.15.3a DS-UWB system	19
Figure 2.6	Packet structure of IEEE 802.15.3a DS-UWB system	19
Figure 2.7	Transmitter architecture of IEEE 802.15.3a DS-UWB system	20
Figure 2.8	Realization of the scrambler linear feedback shift registers of IEEE 802.15.3a DS-UWB system	20
Figure 2.9	Convolutional encoder structure for IEEE 802.15.3a DS-UWB system with (a) constraint length $K=6$ (mandatory) (b) constraint length $K=4$ (optional)	21
Figure 2.10	Convolutional interleaver structure of IEEE 802.15.3a DS-UWB system.....	21
Figure 2.11	Piconet elements of IEEE 802.15.3 system	22
Figure 2.12	Piconet superframe of IEEE 802.15.3 system	22
Figure 3.1	Simulation of passband system in terms of equivalent complex baseband system.....	43
Figure 3.2	Superposition of 100 impulse responses based on the CM3 channel model (NLOS up to 10 m with average RMS delay spread of 15 ns).....	44
Figure 3.3	Average power decay profile for the channel model CM3 (NLOS up to 10 m with average RMS delay spread of 15 ns).	45

Figure 3.4	IEEE 802.15.3a DS-UWB receiver working flow.....	46
Figure 3.5	Proposed receiver architecture of IEEE 802.15.3a DS-UWB system	46
Figure 3.6	Code acquisition structure of IEEE 802.15.3a DS-UWB system.....	47
Figure 3.7	Conventional early-late code tracking loop architecture	47
Figure 3.8	Comparison between early and late edges for the detecting path.....	48
Figure 3.9	Comparison between early and late edges under dense multipaths environment	48
Figure 3.10	Structure of cancellation mechanism for IEEE 802.15.3a DS-UWB system.....	49
Figure 3.11	Proposed code tracking loop with multipath cancellation scheme for IEEE 802.15.3a DS-UWB system.....	49
Figure 3.12	Proposed automatic frequency control loop architecture for IEEE 802.15.3a DS-UWB system	50
Figure 3.13	Decision feedback equalizer architecture	50
Figure 3.14	Average power decay profile for different situations (a) CM1 and CM2 (b) CM3 and CM4.....	51
Figure 3.15	BER performances of DS-UWB system with 110 Mbps data rate under different environments (CM1 to CM4).....	52
Figure 3.16	PER performances of DS-UWB system with 110 Mbps data rate under different environments (CM1 to CM4).....	53
Figure 3.17	BER performances of DS-UWB system with 220 Mbps data rate under different environments (CM1 to CM4).....	54
Figure 3.18	PER performances of DS-UWB system with 220 Mbps data rate under different environments (CM1 to CM4).....	55
Figure 3.19	BER performances of DS-UWB system with 500 Mbps data rate under different environments (CM1 to CM4).....	56
Figure 3.20	PER performances of DS-UWB system with 500 Mbps data rate under different environments (CM1 to CM4).....	57

Figure 4.1	Block diagram of the Rake system	70
Figure 4.2	Rake combining concept.....	70
Figure 4.3	Block diagram of the Pre-Rake system.....	71
Figure 4.4	Pre-Rake combining concept	71
Figure 4.5	A concept of the S-Pre-Rake diversity combining.....	72
Figure 4.6	Ratio of desired path power to ISI path power P_D/P_{ISI} VS finger numbers.....	73
Figure 4.7	PCMC DFE structure.....	73
Figure 4.8	MSE of different channel estimation methods under different environments (a) CM1 (b) CM2 (c) CM3 (d) CM4.....	74
Figure 4.9	BER performances of DS-UWB system of 110 Mbps data rate in CM3 by using S-Pre-Rake diversity combining and different equalizer types compared with high complexity equalizer.....	76
Figure 4.10	BER performances of DS-UWB system of 110 Mbps data rate in CM4 by using S-Pre-Rake diversity combining and different equalizer types compared with high complexity equalizer.....	77
Figure 4.11	BER performances of DS-UWB system of 220 Mbps data rate in CM3 by using S-Pre-Rake diversity combining and different equalizer types compared with high complexity equalizer.....	78
Figure 4.12	BER performances of DS-UWB system of 220 Mbps data rate in CM4 by using S-Pre-Rake diversity combining and different equalizer types compared with high complexity equalizer.....	79

List of Tables

Table 2.1	Piconet channel numbers, chip rates and spreading code sets of IEEE 802.15.3a DS-UWB system.....	23
Table 2.2	Length 24 and 12 spreading codes for BPSK and acquisition of IEEE 802.15.3a DS-UWB system.....	23
Table 2.3	Length 6 and shorter spreading codes for BPSK of IEEE 802.15.3a DS-UWB system.....	24
Table 2.4	Length 12 and shorter spreading codes for 4-BOK, code sets 1 through 6 of IEEE 802.15.3a DS-UWB system.....	24
Table 2.5	Available data rates using BPSK in the lower operating band for IEEE 802.15.3a DS-UWB system.....	25
Table 2.6	Available data rates using 4-BOK in the lower operating band for IEEE 802.15.3a DS-UWB system.....	25
Table 2.7	Available data rates using BPSK in the higher operating band for IEEE 802.15.3a DS-UWB system.....	26
Table 2.8	Available data rates using 4-BOK in the higher operating band for IEEE 802.15.3a DS-UWB system.....	26
Table 2.9	Scrambler seed selection in IEEE 802.15.3a DS-UWB system	27
Table 2.10	FEC code type in IEEE 802.15.3a DS-UWB system	27
Table 3.1	Multipath channel target characteristics and model parameters.	58
Table 3.2	Equalizer taps numbers for different environments.....	58
Table 4.1	S-Pre-Rake finger numbers requirement for different environments. ...	80
Table 4.2	Equalizer taps numbers of proposed joint design system for different environments.....	80

Acronym Glossary

4-BOK	quaternary bi-orthogonal keying
ADC	analog-to-digital conversion
AFC	automatic frequency control
AGC	automatic gain control
AWGN	additive white Gaussian noise
BER	bit error rate
BPSK	binary phase shift keying
CAP	contention access period
CDM	code division multiplexing
CCA	clear channel assessment
CSMA/CA	carrier sense multiple access with collision avoidance
CTAs	channel time allocations
CTAP	channel time allocation period
DAC	digital-to-analog conversion
DFE	decision feedback equalizer
DS-UWB	direct sequence ultrawideband
DSSS	direct sequence spread spectrum
EL	early-late
FBF	feedback filter
FCC	Federal Communications Commission

FDM	frequency division multiplexing
FEC	forward error correction coding
FFF	feed forward filter
FFT	fast Fourier transform
GPS	global positioning system
IEEE	institute of electrical and electronics engineers
IF	intermediate frequency
ISI	inter-symbol interference
LAN	local area network
LOS	line of sight
MAC	medium access control
MB OFDM	multiband orthogonal frequency division multiplexing
MCTAs	management CTAs
MMSE	minimum mean square error
MPCs	multipath components
NBI	narrowband interference
NLOS	non-LOS
OFDM	orthogonal frequency division multiplexing
PAC	piconet acquisition code
PAPR	peak to average power ratio
PCMC	post-cursor multipath cancellation
PER	packet error rate
PHY	physical layer
PN	pseudonoise
PNC	piconet controller
PRBS	pseudo-random binary sequence

PSD	power spectral density
QoS	quality of service
RF	radio frequency
RX	receiver
S-Pre-Rake	selective-Pre-Rake
S-V	Saleh-Valenzuela
SC	sidelobe cancellation
SFD	start frame delimiter
SNR	signal-to-noise ratio
TDM	time division multiplexing
TDMA	time division multiple access
TED	timing error detector
TX	transmitter
UWB	ultrawideband
WPAN	wireless personal-area network
WLAN	wireless LAN



Notations

B	bandwidth of the chip sequence
B_e	bandwidth expansion factor
L	channel length
E_b	bit energy
N_c	processing gain
P_D	useful power
P_{ISI}	ISI power
P_{noise}	noise power
P_{signal}	signal power
R_b	bit rate
T_c	chip duration
T_s	symbol duration
X	the lognormal shadowing
α	multipath gain coefficient
$\beta_{k,l}$	fading associated with the k^{th} ray of the l^{th} cluster
Γ	cluster decay factor
γ	ray decay factor
Λ	cluster arrival rate
λ	ray arrival rate
ρ_0	SNR
σ^2	noise power
τ_κ	delay of the k^{th} multipath component
ξ_l	fading associated with the l^{th} cluster



Chapter 1

Introduction

Ultrawideband (UWB) is a new emerging radio design coming from the fundamental physical benefits of radios designed to use coherent wide-relative-bandwidth propagation [1]. Such systems with ultra-short (nanosecond scale) waveforms can be free of intermediate frequency (IF) processing since they can operate at the baseband. While the base pulses with ultra-short duration have UWB spectral occupancy, UWB radios bring unique advantages that have long been appreciated by the radar and communications communities:

1. Enhanced capability to penetrate through barrier.
2. Ultra high ranging precision at the centimeter level.
3. Supporting very high transmission data rate.
4. Low complexity and transmission power.

The Federal Communications Commission (FCC) has allocated 7,500 MHz of spectrum for unlicensed use of ultra-wideband devices in the 3.1 to 10.6 GHz frequency band [2]. The FCC defines UWB to be signals that occupy more than 500 MHz bandwidth or has a fractional bandwidth of more than 20%. The fractional bandwidth is defined as B/f_c , where $B = f_H - f_L$ denotes the -10 dB bandwidth and

center frequency $f_c = (f_H + f_L)/2$ with f_H being the upper frequency of the -10 dB emission point, and f_L the lower frequency of the -10 dB emission point. According to [1]-[3], UWB systems with $f_c > 2.5$ GHz need to have a -10 dB bandwidth of at least 500 MHz, while UWB systems with $f_c < 2.5$ GHz need to have fractional bandwidth of at least 0.20.

For wireless communications in particular, the power spectral density (PSD) of UWB communication devices should be regulated below -41.25 dBm/MHz by FCC, which allows UWB technology to coexist with services such as the global positioning system (GPS) and the IEEE 802.11 wireless local area networks (WLANs) in the 3.6-10.1 GHz band. Major efforts are currently under way by the IEEE 802.15 Working Group for standardizing UWB wireless radios for indoor multimedia transmissions. Similar to the frequency reuse principle exploited by wireless cellular architectures, low power, short-range UWB communications are also potentially capable of supporting high spatial capacity. Besides, UWB connectivity is anticipated offering a lot of software-controllable parameters that can be used to design location-aware communication networks flexible to scale in rates and power requirements.

UWB technology is emerging as a solution for the IEEE 802.15.3a (TG3a) standard [4]. The purpose of this standard is to provide a specification for a low complexity, low-cost, low power, and high data-rate wireless communication. The data rate must be high enough (greater than 110 Mb/s) to satisfy a set of consumer multimedia industry needs for wireless personal-area network (WPAN) communications. The standard also addresses the quality of service (QoS) capabilities required to support multimedia data types. Products compliant with this standard are envisioned to complement, not compete with, products compliant with IEEE 802.11 [5]. IEEE 802.11 is a standard for local-area networks (LANs), while

TG3a will be a standard for WPANs. The difference is similar to the differences between the Ethernet [6] LAN standard and the USB [7] or Firewire [8] standards that provide for connectivity to peripheral devices.

UWB systems can be divided into two groups: direct sequence spread spectrum impulse radio (DS-UWB) [9]-[11] and multiband orthogonal frequency division multiplexing (MB OFDM) [12]-[15]. In DS-UWB, the pulses are transmitted continuously using a pseudorandom sequence for the spreading of information bits. MB OFDM divides the spectrum into several bands and transmits OFDM symbol in all bands.

This thesis is organized as follows. In Chapter 2, we address the specification and the transmitter architecture of IEEE 802.15.3a DS-UWB system. In Chapter 3, we give a detailed description of channel environment and receiver architecture including all block function, especially focus on the difference compared to conventional direct sequence system. Afterwards, a less complex transceiver with Pre-Rake diversity combining scheme will be proposed in Chapter 4. Finally, we conclude this thesis and propose some potential future works in Chapter 5.

Chapter 2

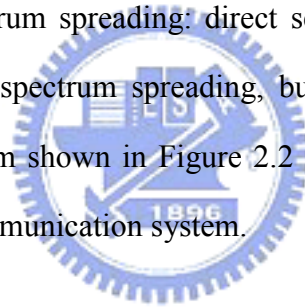
Overview of IEEE 802.15.3a DS-UWB System

The FCC requires that UWB devices occupy a band in the 3.1-10.6 GHz band, according to the spectrum mask in Figure 2.1 [2]. The PSD measured must not exceed the specified -41.25 dBm/MHz. This leads a serious challenge to any UWB system because other services sharing the same band of operation on licensed or unlicensed bands are likely to have a much higher transmit power and, therefore, would subject UWB receivers to considerable interference. The proposed UWB system uses direct sequence modulation to achieve the UWB definition established by FCC. In this chapter, we will give a review of direct sequence technique in Section 2.1. Next, the specification of IEEE 802.15.3a DS-UWB system and all of the transmitter function blocks will be addressed in Section 2.2.

2.1 Review of Direct Sequence Spread Spectrum System

The initial application of spread spectrum (SS) technique was in the development of military communication system [16][17]. At the end of World War II, spectrum spreading with anti-jamming ability was already a familiar concept to radar engineers. During subsequent years, spread spectrum investigation was motivated primarily by the desire to achieve highly jamming resistant communication systems.

By definition, a spread-spectrum system uses a process other than the information signal to spread, or expand, the bandwidth of the signal. There are two fundamental types of spectrum spreading: direct sequence and frequency hopping. These achieve the desired spectrum spreading, but that is about all they have in common. The block diagram shown in Figure 2.2 illustrates the basic element of a spread spectrum digital communication system.



2.1.1 Direct Sequence Spread Spectrum

In a direct sequence spread spectrum (DSSS) communication system [18][19], we assume that the information bit rate at the input to the modulator is R bits/s and the available channel bandwidth is W Hz. In order to utilize the whole available channel bandwidth, the phase of the carrier is shifted pseudorandomly according to the pattern from the pseudonoise (PN) generator at a rate W times/s. The reciprocal of W , denoted by T_c is called the chip interval. The pulse is the basic element in a DS spread spectrum signal.

If we define $T_b=1/R$ to be the duration of a rectangular pulse corresponding to

the transmission time of an information bit, the bandwidth expansion factor W/R may be expressed as

$$B_e = \frac{W}{R} = \frac{T_b}{T_c} \quad (2.1)$$

In practical, the ratio T_b/T_c is an integer,

$$N_c = \frac{T_b}{T_c} \quad (2.2)$$

which is the number of chips per information bit. N_c is the number of phase shifts that can occur in the transmitted signal during the bit duration $T_b=1/R$. Figure 2.3 illustrates the relationships between the PN signal and the data signal.

Typical spectra for the system illustrated in Figure 2.4 is shown directly below the corresponding blocks. The approximation to the spectrum of a DSSS signal employing BPSK data modulation can be representing the modulated carrier as

$$x_c(t) = Ad(t)c(t) \cos(w_c t + \theta) \quad (2.3)$$

where it is assumed that θ is a random phase uniformly distributed in $[0, 2\pi)$. The autocorrelation function for $x_c(t)$ is

$$R_{x_c}(\tau) = \frac{A^2}{2} R_d(\tau) R_c(\tau) \cos(w_c \tau) \quad (2.4)$$

where $R_d(\tau)$ and $R_c(\tau)$ are the autocorrelation function of the data and spreading code. If they are modeled as random sequences, their autocorrelation functions can be given by

$$R_d(\tau) = \Lambda(\tau/T_b) \quad (2.5)$$

and

$$R_c(\tau) = \Lambda(\tau/T_c) \quad (2.6)$$

respectively. Their corresponding power spectral densities are

$$S_d(f) = T_b \text{sinc}^2(T_b f) \quad (2.7)$$

and

$$S_c(f) = T_c \text{sinc}^2(T_c f) \quad (2.8)$$

respectively, where the width of the main lobe of Equation (2.7) is T_b^{-1} and that of (2.8) is T_c^{-1} .

The power spectral density of $x_c(t)$ can be obtained by taking the Fourier transform of (2.4):

$$S_{x_c}(f) = \frac{A^2}{2} S_d(f) * S_c(f) FT(\cos(w_c \tau)) \quad (2.9)$$

where the * denoted convolution. Since the spectral width of $S_d(f)$ is much less than for $S_c(f)$, the convolution of these two spectral is approximately $S_c(f)$. Thus the spectrum of the DSSS modulated signal can be approximated by

$$\begin{aligned} S_{x_c}(f) &= \frac{A^2}{4} [S_c(f - f_c) + S_c(f + f_c)] \\ &= \frac{A^2 T_c}{4} \left\{ \text{sinc}^2 [T_c (f - f_c)] + \text{sinc}^2 [T_c (f + f_c)] \right\} \end{aligned} \quad (2.10)$$

The spectrum is approximately independent of the data spectrum and has a null-to-null bandwidth around the carrier of $2/T_c$ Hz.

2.2 IEEE 802.15.3a DS-UWB System

The DS-UWB system provides a wireless PAN with data payload communication capabilities from 28 to 1320 Mbps. The proposed UWB system employs direct sequence spreading of binary phase shift keying (BPSK) and

quaternary bi-orthogonal keying (4-BOK) UWB pulses [9]-[11]. Forward error correction coding (FEC) is used with a coding rate of $\frac{1}{2}$ and $\frac{3}{4}$. The baseband reference pulse is a root raised cosine low pass filter with 30% excess bandwidth. The implemented baseband impulse response must have a normalized peak cross-correlation within 3 dB of this reference pulse. The proposed UWB system also supports operation in two different bands as shown in Figure 2.5, one band nominally occupying the spectrum from 3.1 to 4.85 GHz (the low band), and the other nominally occupying the spectrum from 6.2 to 9.7 GHz (the high band).

There are 6 piconet channels per operating band, for a total of 12 piconet channels listed in Table 2.1. A DS-UWB device is required to implement piconet channels 1-4 for mandatory. Supporting for piconet channels 5-6 in the lower band and channels 7-12 in the higher band is optional. For each piconet channel, there is a designated chip rate (F_{chip}), a center frequency (F_{center}), and a designated set of spreading codes for use with BPSK and 4-BOK. Each piconet has 2 spreading codes for the code lengths $L=24, 12, 6, 4,$ and 2 and only one code for the lengths of $L=1$ and 3 . When using a BPSK data mode, each piconet uses the first spreading code listed in the Table 2.1 for the desired code length. When using the 4-BOK operating modes, both spreading codes are required to modulate the data symbols.

The chip rates, center frequencies and code sets for each piconet channel are listed in Table 2.1. The specific spreading codes that make up each spreading code set are listed in Tables 2.2 and 2.3. The relationship between the chip rates and the carrier frequencies is always a multiple of three. The use of these offset chip rates for the different piconet channels helps to decorrelate the acquisition codes and the data symbols, in addition to facilitating piconet identification during clear channel assessment (CCA).

2.2.1 Modulation for data, header and preamble

The DS-UWB proposal supports data communication using both BPSK (mandatory) and 4-BOK (optional).

BPSK modulation has low-complexity and easy to implement characteristics. Every compliant device will be able to transmit and receive BPSK modulated signals. For some applications, it is useful to use 4-BOK to improve performance. To support these cases, every device is also required to support the transmission of 4-BOK modulated signals. However, it is optional for devices to support the capability to receive and demodulated 4-BOK modulated waveforms. This approach of requiring 4-BOK support for transmit only results in very low additional device complexity (generation of 4-BOK signals requires little additional complexity relative to BPSK) but it also allows implementers to incorporate the additional complexity required to receive 4-BOK signals if they desire to take advantage of the potential performance gains available in certain situations. There are two options available for mapping the 2 bits to the four signals, either Gray coding where adjacent signals have only 1 bit difference between their respective codes or natural coding where the signals are assigned in the usual binary way. The precise details will be shown in Table 2.4.

In the BPSK data modes, each symbol carries only a single data bit. For BPSK modulation, the data bit determines whether the spreading code with the desired length is transmitted with a polarity of either (+1) or (-1).

In the 4-BOK data modes, each symbol carries two data bits. For this mode, modulation is accomplished by dividing the data bit stream into block of two bits, then mapping each block of two bits into one of two possible spreading codes for the desired data symbol rate as well as a polarity of either (+1) or (-1).

The data rates that are available using the lower operating band are listed in Tables 2.5 and 2.6. Each data rate is achieved using the FEC rate and code length listed. Table 2.5 lists those modes available using BPSK modulation. Table 2.6 lists those modes available using 4-BOK modulation. The additional data rates that are available using the higher operating band using BPSK and 4-BOK modulation are listed in Tables 2.7 and 2.8, respectively.

2.2.2 PHY preamble and header components

The general preamble structure

The packet structure is shown in Figure 2.6, which is summarized below:

1. The transmitter (TX) Medium Access Control (MAC) selects one of 6 piconet acquisition codes (PAC) and sets the corresponding carrier offset frequency.
2. The TX modulates the PAC code (one bit per PAC symbol) with random data to generate the acquisition sequence which is used by the receiver for initial estimation like automatic gain control (AGC) and clock frequency lock. There are 3 preamble options that are structurally the same except for field durations:
 - (1). A nominal preamble (15 us) is used for nominal data rates and channels. It is suggested that the first 10 us is used for AGC and timing estimation, the rest 5 us is used for Rake and equalizer training.
 - (2). A long preamble (30 us) is used for extended range applications.
 - (3). A short preamble (5 us) is used in short range and high data rate applications
3. Next is sent the training sequence. The receiver uses this training sequence to adjust the receiver.

4. The TX next sends the start frame delimiter (SFD) that indicates to the receiver (RX) the next frame will be the Physical Layer (PHY) header, which contains rate information.
5. After the PHY header comes the MAC header.
6. Following the MAC header the TX starts sending data frames.

The piconet acquisition codeword (PAC)

There are six PAC codewords, which are given in Table 2.2 above. Each piconet uniquely uses one of these codes. The selection of the code is determined by the piconet controller (PNC) during the initial scan prior to initiating the piconet (the PNC selects a PAC codeword that is not in use). Use of the PAC codewords provides a degree of "channel separation" between overlapping piconets during preamble acquisition, limited only by the rms cross-correlation properties of the PAC codeword set. The PAC codewords ensures that a DEV will train on the preamble associated with the desired piconet. Each PNC number has an associated chipping rate and carrier frequency given in Table 2.1 .

2.2.3 Transmitter Architecture

As show in Figure 2.7, the transmitter architecture of DS-UWB is similar to that of a conventional DS system. In the following section we will introduce the transmitter architecture of DS-UWB in detail.

Data Scrambler

A scrambler shall be employed to ensure an adequate number of bit transitions to support clock recovery. The stream of downlink packets shall be scrambled by modulo-2 addition of the data with the output of the pseudo-random binary sequence (PRBS) generator, as illustrated in Figure 2.8.

The scrambler shall be used for the MAC header and frame body. The PHY preamble and PHY header shall not be scrambled. The polynomial, 1, for the pseudo random binary sequence (PRBS) generator shall be:

$$g(D) = 1 + D^{14} + D^{15} \quad (2.11)$$

where D is a single bit delay element. The polynomial forms not only a maximal length sequence, but also is a primitive polynomial. By the given generator polynomial, the corresponding PRBS, is generated as

$$x_n = x_{n-14} \oplus x_{n-15} \quad (2.12)$$

where + and \oplus denote modulo-2 addition.

The following sequence defines the initialization sequence,

$$x_{init} = [x_{n-1}^i \ x_{n-2}^i \ x_{n-3}^i \ x_{n-4}^i \ x_{n-5}^i \ x_{n-6}^i \ x_{n-7}^i \ x_{n-8}^i \ x_{n-9}^i \ x_{n-10}^i \ x_{n-11}^i \ x_{n-12}^i \ x_{n-13}^i \ x_{n-14}^i \ x_{n-15}^i] \quad (2.13)$$

where x_{n-k}^i represents the binary initial value at the output of the k th delay element.

The scrambled data bits, s_n , are obtained as follows:

$$s_0 = b_0 \oplus x_0 \quad (2.14)$$

where b_n represents the unscrambled data bits. The side-stream de-scrambler at

the receiver shall be initialized with the same initialization vector, x_{init} , used in the transmitter scrambler. The initialization vector is determined from the seed identifier contained in the PHY header of the received packet.

The 15 bit seed value chosen shall correspond to the seed identifier, shown in Table 2.9. The seed identifier value is set to 00 when the PHY is initialized and is incremented in a 2-bit rollover counter for each packet that is sent by the PHY. The value of the seed identifier that is used for the packet is sent in the PHY header.

Forward Error Correction Coding

The convolutional encoder is used to encode data so that the decoder can correct errors introduced by noise and interference in the channel. Two important characteristics of a convolutional encoder are its code rate and constraint length. If k data bits are shifted in for every n encoded bits shifted out, the code rate equals k/n . If the maximum degree of the generator polynomials are m , then the constraint length of the code equals $k(m+1)$. A half-rate convolutional encoder is a linear feed-forward shift register network in which, for every data bit that is shifted in, two encoded bits are generated. For each of the two codes specified in Table 2.10, the basic code is a 1/2 rate code that can be punctured to achieve a code rate of 3/4 at slightly less coding gain. And two types of convolutional encoder structure with different constraint length are shown in Figure 2.9.

Convolutional Interleaver for Coded Bits

The convolutional decoder is sensitive to burst errors; hence, interleaving is used to disperse burst errors. Convolutional interleaving is used over block interleaving because of it has lower latency and memory requirements. The structure

for a convolutional interleaver is shown below in Figure 2.10. The encoded bits are sequentially shifted in to the bank of N registers; each successive register provides J bits more storage than did the preceding. The zeroth register provides no storage. With each new code bit the commutator switches to a new register, and the new code bit is shifted in while the oldest code bit in that register is shifted out. After the $(N-1)$ th register, the commutator returns to the zeroth register and starts again. The deinterleaver performs the inverse operation. This is exactly the same except that the delays are reversed i.e. the first delay is $(N-1)J$ and the last delay is 0. The input and output commutators for both interleaving and deinterleaving must be synchronized. The bit interleaver shall have the values of $J=7$ and $N=10$.

2.2.4 Multiple Access Scheme

DS-UWB provides frequency division multiplexing (FDM), code division multiplexing (CDM), and time division multiplexing (TDM) to support multiple access.

1. **FDM** : Choice of one of two operating frequency bands as shown in Figure 2.5.
2. **CDM** : 6 code sets available within each frequency band.

FDM and CDM can both be used to achieve multiple access between different piconet. A piconet is a wireless ad hoc data communications system which allows a number of independent data devices to communicate with each other. Piconet is distinguished from other types of data networks in that communications are normally confined to a small area around person or object that typically covers at least 10 m in all directions and surround the person or a thing whether stationary or in motion.

An 802.15.3a piconet consists of several components, as shown in Figure 2.11.

The basic component is the devices. One device is required to assume the role of the PNC of the piconet. The PNC provides the basic timing for the piconet with the beacon. Additionally, the PNC manages the QoS requirements, power save modes and access control to the piconet.

3. **TDM** : Within each piconet the 802.15.3 time division multiple access (TDMA) protocol is used.

Timing in the 802.15.3 piconet is based on the superframe, which is illustrated in Figure 2.12. The superframe is composed of three parts:

- (1). The beacon, which is used to set the timing allocations and to communicate management information for the piconet. The beacon consists of the beacon frame, as well as any announce commands sent by the PNC as a beacon extension.
- (2). The contention access period (CAP), which is used to communicate commands and/or asynchronous data if it is present in the superframe.
- (3). The channel time allocation period (CTAP), which is composed of channel time allocations (CTAs), including management CTAs (MCTAs). CTAs are used for commands, isochronous streams and asynchronous data connections.

The length of the CAP is determined by the PNC and communicated to the DEVs in the piconet via the beacon. However, the PNC is able to replace the functionality provided in the CAP with management CTAs (MCTAs). MCTAs are a type of CTA that is used for communications between the DEVs and the PNC. The CAP uses carrier sense multiple access with collision avoidance (CSMA/CA) for the medium access. The CTAP, on the other hand, uses a standard TDMA protocol where the DEVs have specified time windows. MCTAs are either assigned to a specific source/destination pair and use TDMA for access or they are shared CTAs that are accessed using the slotted aloha protocol.

2.3 Summary

Specification of IEEE 802.15.3a system has been introduced in this chapter. Compared to other DS systems, although the transmitter architecture is similar to conventional DS system like IEEE 802.11b, the transmitted ultra short pulse will induce difference to the channel impulse response and conventional receiver function blocks should be modified. More technical details will be discussed in Chapter 3.



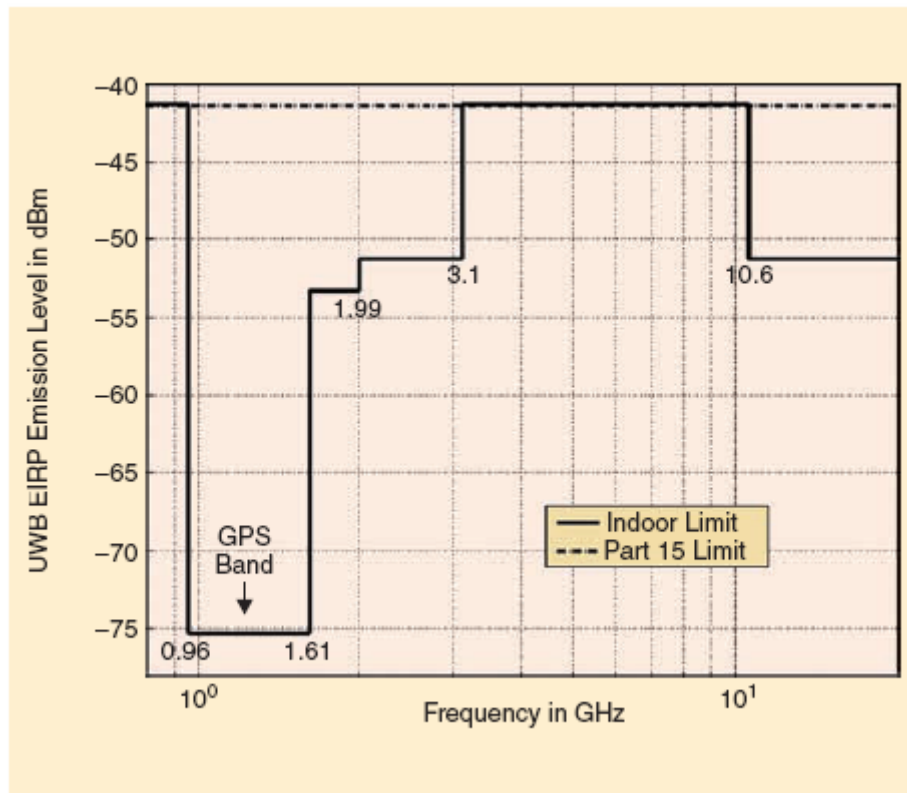


Figure 2.1 UWB spectral mask for indoor communication system

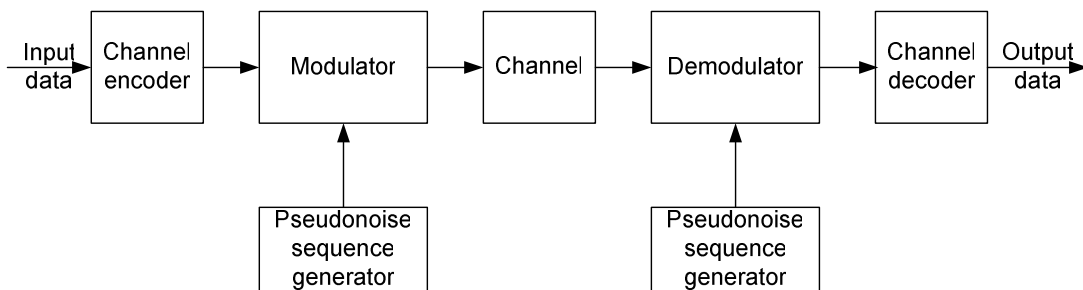


Figure 2.2 Model of spread spectrum digital communication system

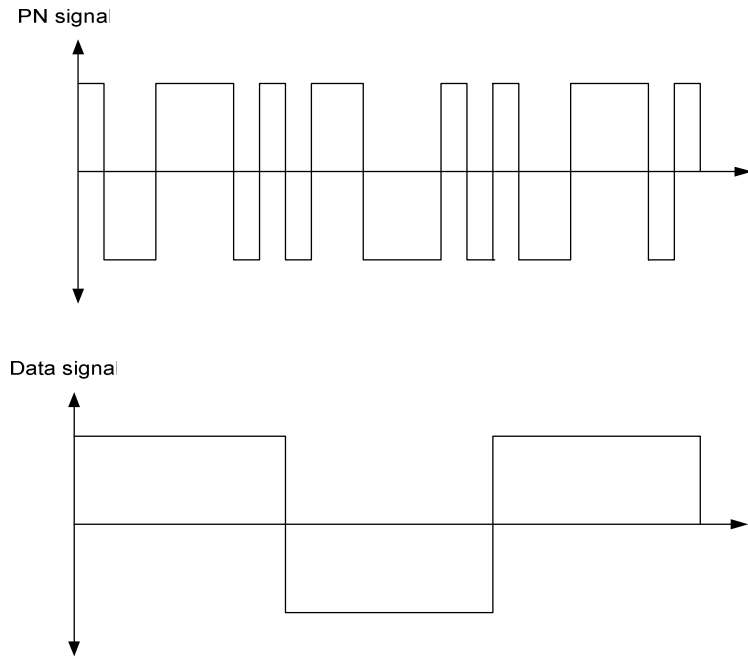


Figure 2.3 PN and data signal

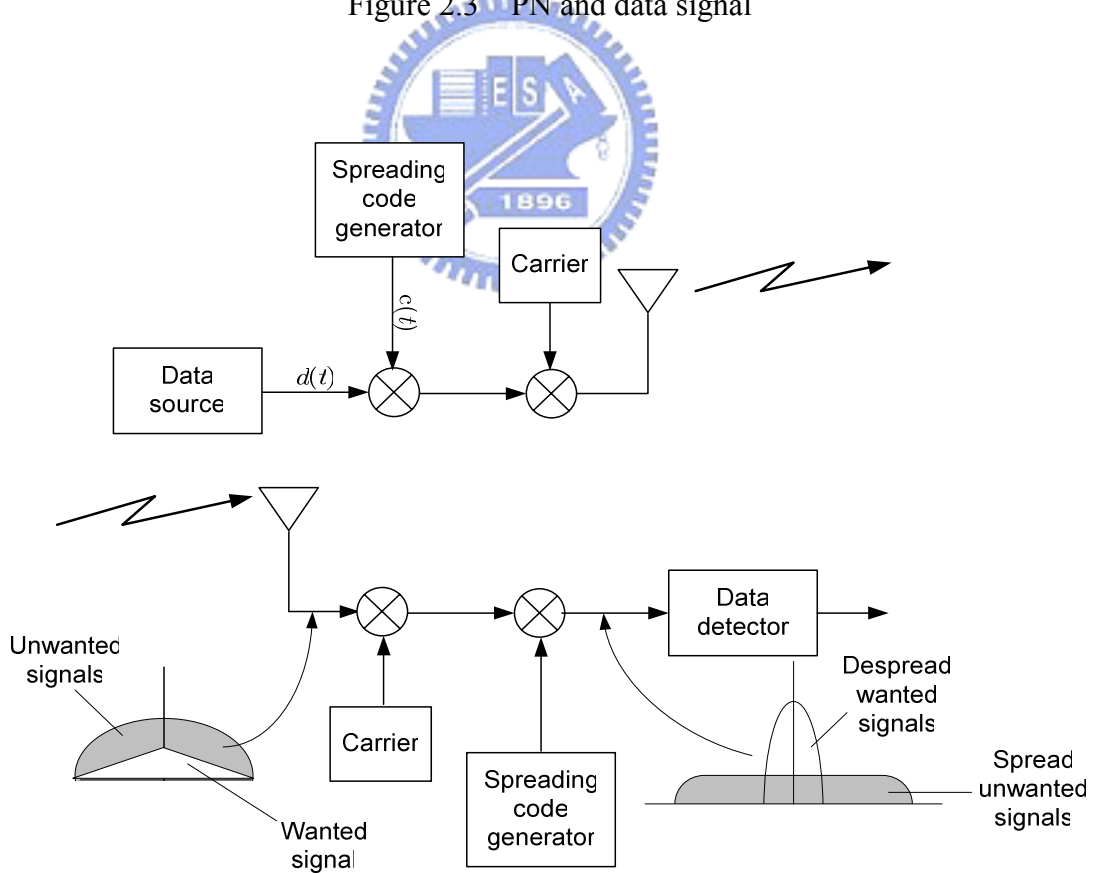


Figure 2.4 Block diagram of a DSSS communication system

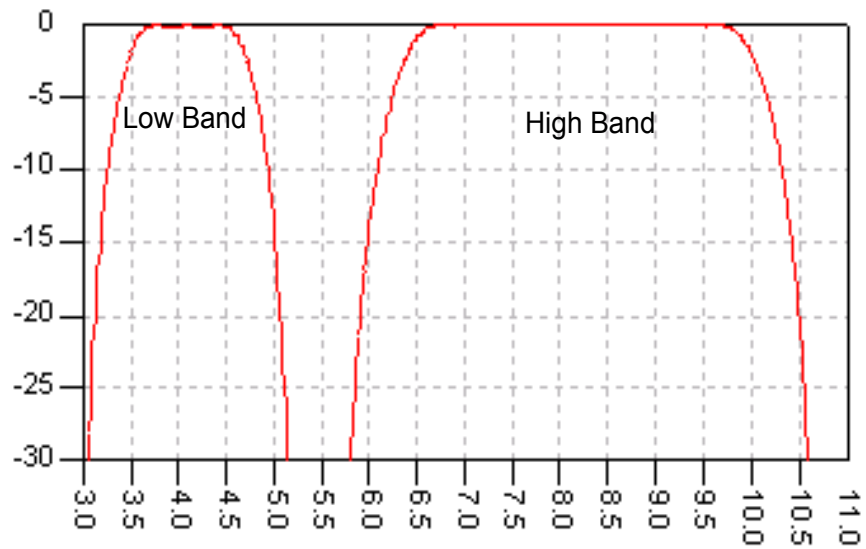


Figure 2.5 Spectrum mask of IEEE 802.15.3a DS-UWB system

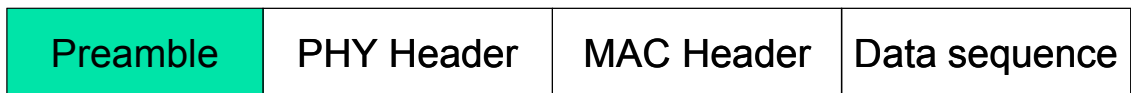


Figure 2.6 Packet structure of IEEE 802.15.3a DS-UWB system

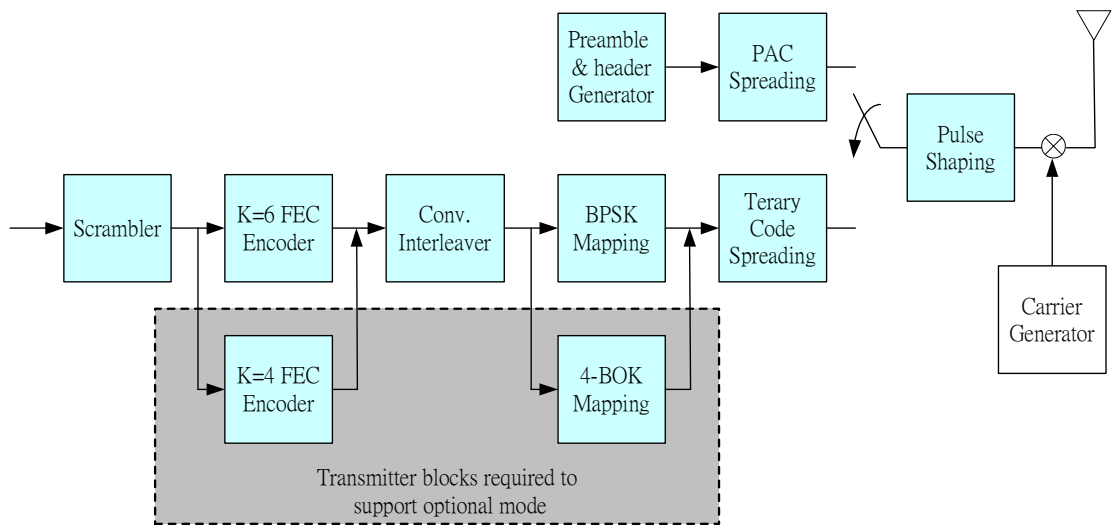


Figure 2.7 Transmitter architecture of IEEE 802.15.3a DS-UWB system

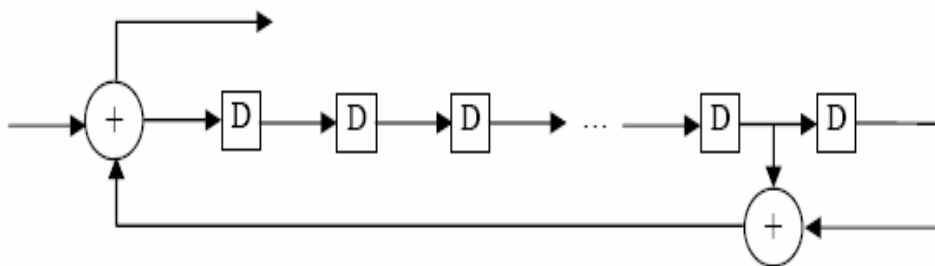
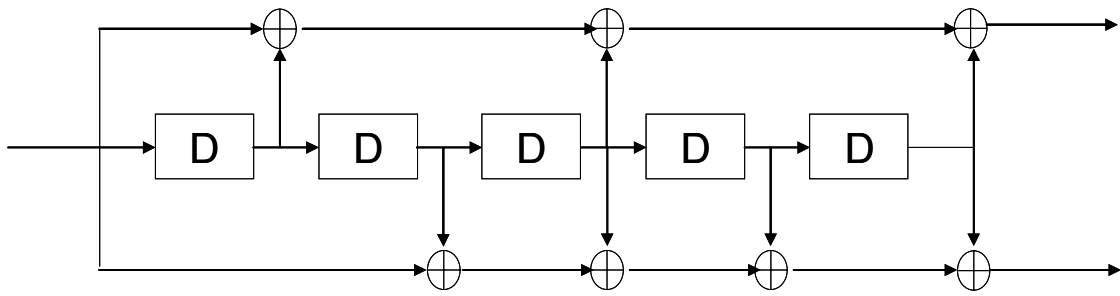
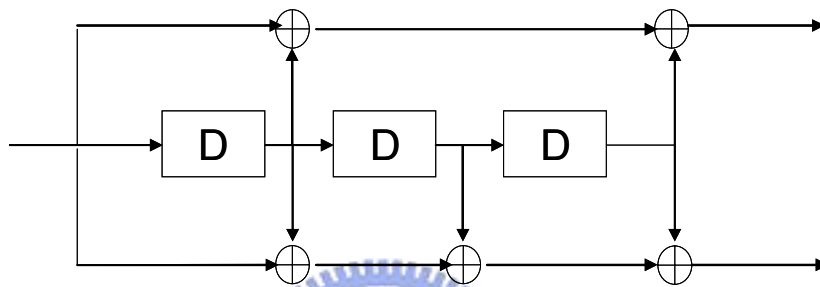


Figure 2.8 Realization of the scrambler linear feedback shift registers of IEEE 802.15.3a DS-UWB system



(a)



(b)

Figure 2.9 Convolutional encoder structure for IEEE 802.15.3a DS-UWB system with (a) constraint length $K=6$ (mandatory) (b) constraint length $K=4$ (optional)

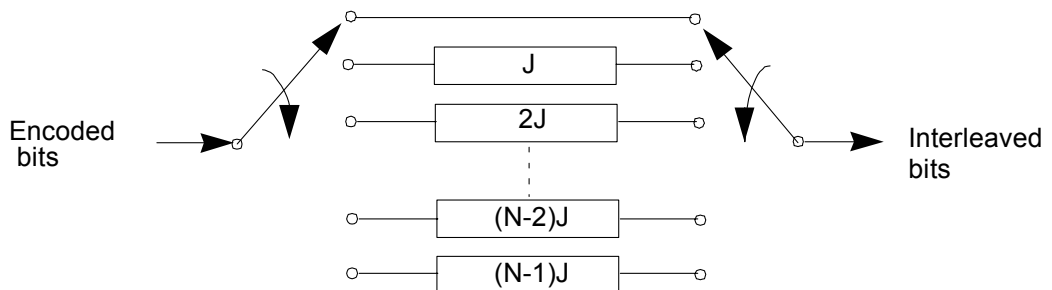


Figure 2.10 Convolutional interleaver structure of IEEE 802.15.3a DS-UWB system

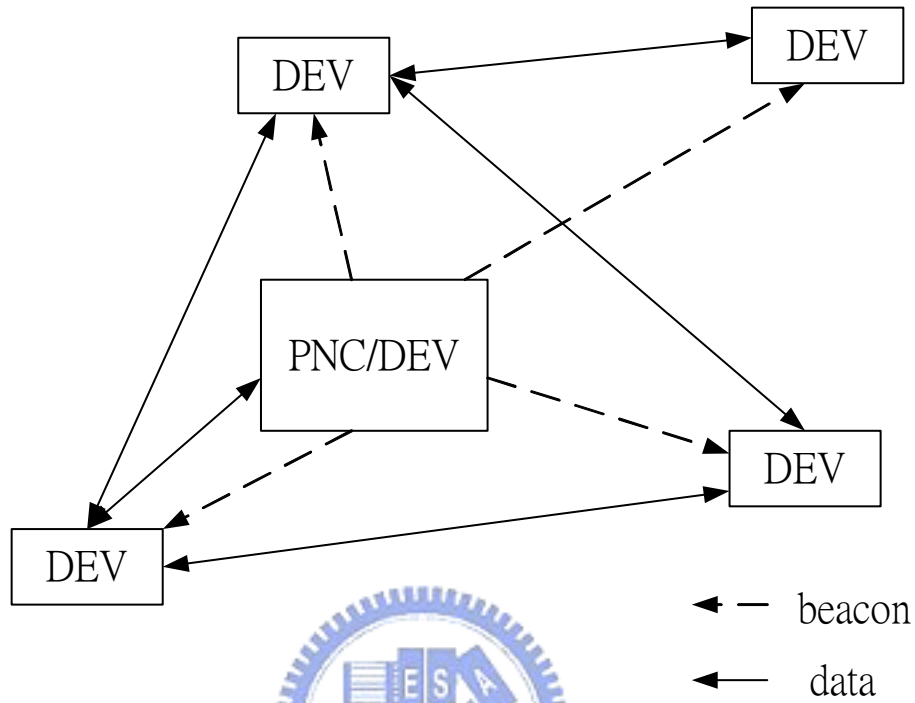


Figure 2.11 Piconet elements of IEEE 802.15.3 system

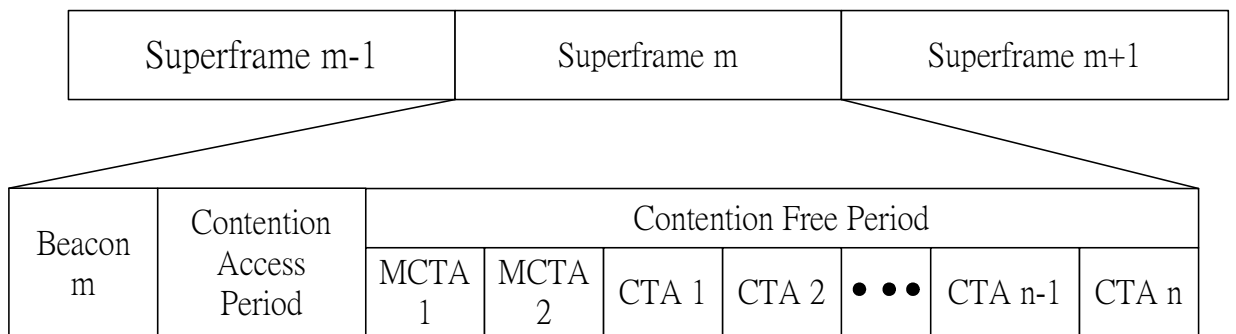


Figure 2.12 Piconet superframe of IEEE 802.15.3 system

Table 2.1 Piconet channel numbers, chip rates and spreading code sets of IEEE 802.15.3a DS-UWB system

Piconet Channel	Chip Rate	Center Frequency	Spreading Code Set
1	1313 MHz	3939 MHz	1
2	1326 MHz	3978 MHz	2
3	1339 MHz	4017 MHz	3
4	1352 MHz	4056 MHz	4
5	1300 MHz	3900 MHz	5
6	1365 MHz	4094 MHz	6
7	2626 MHz	7878 MHz	1
8	2652 MHz	7956 MHz	2
9	2678 MHz	8034 MHz	3
10	2704 MHz	8112 MHz	4
11	2600 MHz	7800 MHz	5
12	2730 MHz	8190 MHz	6

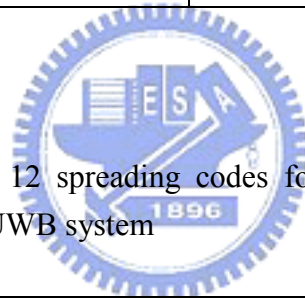


Table 2.2 Length 24 and 12 spreading codes for BPSK and acquisition of IEEE 802.15.3a DS-UWB system

Code Set	$L=24$	$L=12$
1	-1, 0, 1, -1, -1, -1, 1, 1, 0, 1, 1, 1, 1, -1, 1, -1, 1, 1, 1, -1, 1, -1, -1, 1	0, -1, -1, -1, 1, 1, 1, -1, 1, 1, -1, 1
2	-1, -1, -1, -1, 1, -1, 1, -1, 1, -1, -1, 1, -1, 1, 1, -1, -1, 1, 1, 0, -1, 0, 1, 1	-1, 1, -1, -1, 1, -1, -1, -1, 1, 1, 1, 0
3	-1, 1, -1, -1, 1, -1, -1, 1, -1, 0, -1, 0, -1, -1, 1, 1, 1, -1, 1, 1, 1, -1, -1, -1	0, -1, 1, -1, -1, 1, -1, -1, -1, 1, 1, 1
4	0, -1, -1, -1, -1, -1, -1, 1, 1, 0, -1, 1, 1, -1, 1, -1, -1, 1, 1, -1, 1, -1, 1, 1	-1, -1, -1, 1, 1, 1, -1, 1, 1, -1, 1, 0
5	-1, 1, -1, 1, 1, -1, 1, 0, 1, 1, 1, -1, -1, 1, 1, -1, 1, 1, 1, -1, -1, -1, 0, -1	-1, -1, -1, 1, 1, 1, -1, 1, 1, -1, 1, 0
6	0, -1, -1, 0, 1, -1, -1, 1, -1, -1, 1, 1, 1, 1, -1, -1, 1, -1, 1, -1, 1, 1, 1, 1	0, -1, -1, -1, 1, 1, 1, -1, 1, 1, -1, 1

Table 2.3 Length 6 and shorter spreading codes for BPSK of IEEE 802.15.3a DS-UWB system

Code Set Numbers	$L = 6$	$L = 4$	$L = 3$	$L = 2$	$L = 1$
1 through 6	1,0,0,0,0,0	1,0,0,0	1,0,0	1,0	1



Table 2.4 Length 12 and shorter spreading codes for 4-BOK, code sets 1 through 6 of IEEE 802.15.3a DS-UWB system

Input data: Gray coding (First in time on left)	Input data: Natural coding (First in time on left)	$L = 12$	$L = 6$	$L = 4$	$L = 2$
00	00	1,0,0,0,0,0,0,0,0,0,0,0	1,0,0,0,0,0	1,0,0,0	1, 0
01	01	0,0,0,0,0,0,0,1,0,0,0,0	0,0,0,1,0,0	0,0,1,0	0, 1
11	10	-1,0,0,0,0,0,0,0,0,0,0,0	-1,0,0,0,0,0	-1,0,0,0	-1, 0
10	11	0,0,0,0,0,0,-1,0,0,0,0,0	0,0,0,-1,0,0	0,0,-1,0	0, -1

Table 2.5 Available data rates using BPSK in the lower operating band for IEEE 802.15.3a DS-UWB system

Data Rate	FEC Rate	Code Length	Bits per Symbol	Symbol Rate
28 Mbps	$\frac{1}{2}$	L=24	1	$F_{\text{chip}}/24$
55 Mbps	$\frac{1}{2}$	L=12	1	$F_{\text{chip}}/12$
110 Mbps	$\frac{1}{2}$	L=6	1	$F_{\text{chip}}/6$
220 Mbps	$\frac{1}{2}$	L=3	1	$F_{\text{chip}}/3$
500 Mbps	$\frac{3}{4}$	L=2	1	$F_{\text{chip}}/2$
660 Mbps	1	L=2	1	$F_{\text{chip}}/2$
1000 Mbps	$\frac{3}{4}$	L=1	1	F_{chip}
1320 Mbps	1	L=1	1	F_{chip}

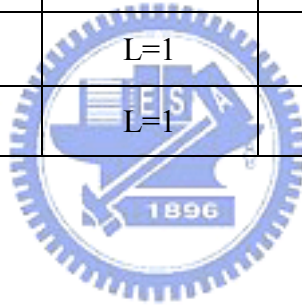


Table 2.6 Available data rates using 4-BOK in the lower operating band for IEEE 802.15.3a DS-UWB system

Data Rate	FEC Rate	Code Length	Bits per Symbol	Symbol Rate
110 Mbps	$\frac{1}{2}$	L=12	2	$F_{\text{chip}}/12$
220 Mbps	$\frac{1}{2}$	L=6	2	$F_{\text{chip}}/6$
500 Mbps	$\frac{3}{4}$	L=4	2	$F_{\text{chip}}/4$
660 Mbps	1	L=4	2	$F_{\text{chip}}/4$
1000 Mbps	$\frac{3}{4}$	L=2	2	$F_{\text{chip}}/2$
1320 Mbps	1	L=2	2	$F_{\text{chip}}/2$

Table 2.7 Available data rates using BPSK in the higher operating band for IEEE 802.15.3a DS-UWB system

Data Rate	FEC Rate	Code Length	Bits per Symbol	Symbol Rate
55 Mbps	$\frac{1}{2}$	L=24	1	$F_{\text{chip}}/24$
110 Mbps	$\frac{1}{2}$	L=12	1	$F_{\text{chip}}/12$
220 Mbps	$\frac{1}{2}$	L=6	1	$F_{\text{chip}}/6$
500 Mbps	$\frac{3}{4}$	L=4	1	$F_{\text{chip}}/4$
660 Mbps	1	L=4	1	$F_{\text{chip}}/4$
1000 Mbps	$\frac{3}{4}$	L=2	1	$F_{\text{chip}}/2$
1320 Mbps	1	L=2	1	$F_{\text{chip}}/2$



Table 2.8 Available data rates using 4-BOK in the higher operating band for IEEE 802.15.3a DS-UWB system

Data Rate	FEC Rate	Code Length	Bits per Symbol	Symbol Rate
220 Mbps	$\frac{1}{2}$	L=12	2	$F_{\text{chip}}/12$
660 Mbps	$\frac{3}{4}$	L=6	2	$F_{\text{chip}}/6$
1000 Mbps	$\frac{3}{4}$	L=4	2	$F_{\text{chip}}/4$
1320 Mbps	1	L=4	2	$F_{\text{chip}}/4$

Table 2.9 Scrambler seed selection in IEEE 802.15.3a DS-UWB system

Seed Identifier	Seed Value
0,0	1111 1111 1111 111
0,1	0111 0000 1111 111
1,0	0111 1111 0000 000
1,1	0111 1000 0000 111



Table 2.10 FEC code type in IEEE 802.15.3a DS-UWB system

Code Type	Constraint Length & Generator Polynomials	Possible Rates	Implementation Requirements
Convolutional	Constraint length $K = 6$, Generating polynomial (65, 57)	Rate $\frac{1}{2}$ or $\frac{3}{4}$	Mandatory for Tx: Rate $\frac{1}{2}$ & $\frac{3}{4}$ Mandatory for Rx: Rate $\frac{1}{2}$ Optional for Rx: Rate $\frac{3}{4}$
Convolutional	Constraint length $K = 4$, Generating polynomial (15,17)	Rate $\frac{1}{2}$ or $\frac{3}{4}$	Mandatory for Tx: Rate $\frac{1}{2}$ & $\frac{3}{4}$ Optional for Rx: Rate $\frac{1}{2}$ & $\frac{3}{4}$

Chapter 3

Performance of IEEE 802.15.3a DS-UWB System

The architecture of IEEE 802.15.3a DS-UWB system will be described in this chapter. Due to the extremely wide bandwidth, the fine resolution characteristic will induce new effects. Hence conventional indoor channel models and some receiver algorithms are not suitable anymore. The rest of this chapter is organized as follows. Indoor UWB channel model will be described in Section 3.1. Synchronization techniques for IEEE 802.15.3a DS-UWB system will be introduced in Section 3.2. Channel equalization algorithm will be developed in Section 3.3. Finally, performance simulations are shown in Section 3.4.

3.1 Indoor UWB Channel Model

Wireless propagation channels have been studied for more than 50 years, and a large number of channel models are already available. The signal that has propagated through a wireless channel consists of multiple echoes of the originally transmitted signal; this phenomenon is known as multipath propagation. The different multipath components (MPCs) are characterized by different attenuations and delays. The

correct modeling of the parameters describing the MPCs is the key point of channel modeling.

In UWB systems, the intended radiation can cover a bandwidth closed to 10 GHz, and the unintended radiation can cover an even larger frequency range. This large bandwidth can give rise to new effects. For example, only few multipath components overlap within each resolvable delay bin, hence the central limit theorem is no longer suitable, and the amplitude fading statistics are not Rayleigh distributed. Also, there can be delay bins into which no MPCs fall, and thus are empty. It then becomes necessary to characterize the likelihood that this happens, and that an empty bin is followed by a full one. For a realistic performance assessment, a UWB channel model like the 802.15.3a standard model has to include all those effects.

Three main indoor channel models were considered here: the tap-delay line Rayleigh fading model [21], the Saleh-Valenzuela (S-V) model [22], and the Δ -K model described in [23], as well as several novel modifications to these approaches that better matched the measurement characteristics. Each channel model was parameterized in order to best fit the important channel characteristics described above. Although many good models were contributed to the group, the model finally adopted was based on a modified S-V model that seemed to best fit the channel measurements. In particular, the channel measurements showed multipath arrivals in clusters rather than in a continuum, as is customary for narrowband channels.

3.1.1 Saleh-Valenzuela Model

The S-V model was proposed in [22] to model the multipath of an indoor environment for wideband channels on the order of 100 MHz. Even at this relatively narrow bandwidth, a clustering phenomenon was observed in the channel. In order to

capture this effect, the authors proposed an approach that modeled the multipath arrival times using a statistically random process based on the Poisson process. In other words, the interarrival time of multipath components is exponentially distributed. In addition, the multipath arrivals were grouped into two different categories: a cluster arrival and a ray arrival within a cluster, there are 6 key parameters that define the model [24]:

Λ = cluster arrival rate;

λ = ray arrival rate, i.e., the arrival rate of path within each cluster;

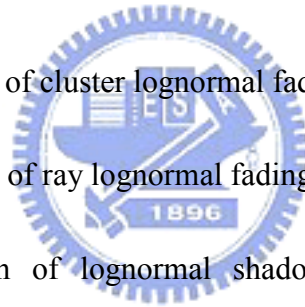
Γ = cluster decay factor;

γ = ray decay factor;

σ_1 = standard deviation of cluster lognormal fading term (dB).

σ_2 = standard deviation of ray lognormal fading term (dB).

σ_x = standard deviation of lognormal shadowing term for total multipath realization (dB).



Multipath model

The amplitude statistics in the original S-V model were found to best match the Rayleigh distribution, the power of which is controlled by the cluster and ray decay factors. However, the measurements in UWB channels indicated that the amplitudes do not follow a Rayleigh distribution. Rather, either a lognormal or Nakagami distribution can fit the data equally well, which has been validated using Kolmogorov-Smirnov testing with a 1 percent significance level. Based on these results, the S-V model was modified for the IEEE model by prescribing a lognormal

amplitude distribution. The model also includes a shadowing term to account for total received multipath energy variation that results from blockage of the line-of-sight path. The discrete time impulse response multipath model can be given by

$$h_i(t) = X_i \sum_{l=0}^L \sum_{k=0}^K \alpha_{k,l}^i \delta(t - T_l^i - \tau_{k,l}^i) \quad (3.1)$$

where $\{\alpha_{k,l}^i\}$ are the multipath gain coefficient, $\{T_l^i\}$ is the delay of the l th cluster, $\{\tau_{k,l}^i\}$ is the delay of the k th multipath component relative to the l th cluster arrival time (T_l^i) , $\{X_i\}$ represents the log-normal shadowing, and i refers to the i th realization.

By definition, we have $\tau_{0,l} = 0$. The distribution of cluster arrival time and the ray arrival time are given by the independent interarrival exponential probability density function

$$p(T_l | T_{l-1}) = \Lambda \exp[-\Lambda(T_l - T_{l-1})], \quad l > 0 \quad (3.2)$$

$$p(\tau_{k,l} | \tau_{(k-1),l}) = \lambda \exp[-\lambda(\tau_{k,l} - \tau_{(k-1),l})], \quad k > 0 \quad (3.3)$$

The channel coefficients are defined as follows:

$$\alpha_{k,l} = p_{k,l} \xi_l \beta_{k,l}, \quad 20 \log_{10}(\xi_l \beta_{k,l}) \propto \text{Normal}(\mu_{k,l}, \sigma_1^2 + \sigma_2^2) \quad (3.4)$$

where $n_1 \propto \text{Normal}(0, \sigma_1^2)$ and $n_2 \propto \text{Normal}(0, \sigma_2^2)$ are independent and correspond to the fading on each cluster and ray, respectively,

$$E\left[|\xi_l \beta_{k,l}|^2\right] = \Omega_0 e^{-T_l/\Gamma} e^{-\tau_{k,l}/\gamma} \quad (3.5)$$

where T_l is the excess delay of bin l and Ω_0 is the mean energy of the first path of

the first cluster, and $p_{k,l}$ is equiprobable ± 1 to account for signal inversion due to reflections. The $\mu_{k,l}$ is given by

$$\mu_{k,l} = \frac{10 \ln(\Omega_0) - 10T_l/\Gamma - 10\tau_{k,l}/\gamma - (\sigma_1^2 + \sigma_2^2) \ln(10)}{\ln(10)} - \frac{(\sigma_1^2 + \sigma_2^2) \ln(10)}{20} \quad (3.6)$$

In the above equations, ζ_l reflects the fading associated with the l th cluster, and $\beta_{k,l}$ corresponds to the fading associated with the k th ray of the l th cluster.

Finally, since the log-normal shadowing of the total multipath energy is captured by the term, X_i , the total energy contained in the terms $\{\alpha_{k,l}^i\}$ is normalized to unity for each realization. This shadowing term is characterized by $20 \log_{10}(X_i) \propto \text{Normal}(0, \sigma_x^2)$.

Note that, a complex tap model was not adopted here. The complex baseband model is a natural fit for narrowband systems to capture channel behavior independently of carrier frequency, but this motivation breaks down for UWB systems where a real-valued simulation at radio frequency (RF) may be more natural. Figure 3.1 illustrates the equivalent model for simulation of passband system in terms of complex baseband system. Therefore the real-valued passband multipath channel response is simplified as follow

$$h(t) = \sum_{i=0}^{L-1} \alpha_i \delta(t - \tau_i) \quad (3.7)$$

where α_i is the real-values channel coefficient. The equivalent baseband multipath channel response is described by

$$\tilde{h}(t) = \sum_{i=0}^{L-1} \alpha_i e^{-j2\pi f_c \tau_i} \delta(t - \tau_i) = \sum_{i=0}^{L-1} \tilde{\alpha}_i \delta(t - \tau_i) \quad (3.8)$$

The proposed model parameters were designed to fit measurement results, and

Table 3.1 provides the results of this fit for four kinds different channel environments (LOS refers to line of sight, NLOS to non-LOS).

1. CM1 is based on LOS (0 – 4 m) channel measurements.
2. CM2 is based on NLOS (0 – 4 m) channel measurements.
3. CM3 is based on NLOS (4 – 10 m) channel measurements.
4. CM4 is generated to fit a 25 ns RMS delay spread to represent an extreme NLOS multipath channel.

Figures 3.2 and 3.3, along with the channel measurement characteristics listed in Table 3.1, highlight characteristics of the multipath channel that are important to discuss. First, the multipath spans several nanoseconds in time, which results in ISI if UWB pulses are closely spaced in time. However, this interference can be mitigated in a number of ways through proper waveform design as well as signal processing and equalization algorithms. Second, the ultra wide bandwidth of a transmitted pulse results in the ability to individually resolve several multipath components.

3.2 Synchronization Techniques for IEEE

802.15.3a DS-UWB System

The receiver working flow is described in Figure 3.4. Synchronization should be done before the rest work like channel estimation and data demodulation. Here, we consider three steps to complete the initialization of the receiver: (i) code acquisition is used to find packet start time and search all delayed path caused by multipath effect; (ii) code tracking can combat the asynchronous between transmitter and receiver due to the sampling clock error; (iii) automatic frequency control (AFC)

loop is the solution to estimate frequency offset caused by the mismatch of radio frequency (RF) component. The overall proposed receiver architecture is shown in Figure 3.5.

3.2.1 Code Acquisition

Code acquisition is usually achieved a coarse alignment within some fraction of one code-chip interval between two PN codes. Because it is the first synchronization algorithm, the rest of the synchronization process is dependent on good packet detection performed. Fortunately, the preamble of the DS-UWB system has been designed to help the detection of the start edge of the packet. The cross-correlation method takes advantage of the periodicity of the synchronization at the start of the preamble. As shown in Figure 3.6, the matched filter with the coefficient of the preamble sequence is proposed to correlate the received symbols. The preamble sequence is pre-assigned by the piconet channel of MAC layer. When some threshold of correlation is exceeded by the output power of the post-matched filter, the receiver will declare a packet detection.

3.2.2 Code Tracking Loop

Due to the sampling clock error as shown in Figure 3.7, the sampling clock error will cause slow packet shift during the transmission. In conventional DS system, Early-late (EL) code tracking loop is usually used to maintain this asynchronous [25]. Assume the IEEE 802.15.3a DS-UWB transmitter sends known preamble sequence $\{a_n\}$. These data symbols are spread by the spreading factor N_c ($N_c = 24$) using the effective spreading sequence $\{c_v\}$ which is called PAC. The transmitted signal is given by

$$s(t) = \sum_n a_n \sum_{v=0}^{N_c-1} c_v g(t - vT_c) \quad (3.9)$$

where $g(t)$ is the pulse shaping defined in [9], T_c is the chip duration. After the transmitted signal travels through the multipath channel defined in (3.8), the received signal can be described by

$$r(t) = \sum_{l=0}^{L-1} \tilde{\alpha}_l \sum_n a_n \sum_{v=0}^{N_c-1} c_{nN_c+v} R_g(t - vT_c - \tau_l) + n(t) \quad (3.10)$$

where $n(t)$ represents the additive white Gaussian noise (AWGN) filtered by the receiver pulse matched filter, $R_g(t)$ is the combined transmit and receive filter pulse form at the output of the matched filter which is given by

$$R_g(t) = \int_{-\infty}^{\infty} g^*(\tau) g(t + \tau) d\tau \quad (3.11)$$

The conventional EL code tracking loop is shown in Figure 3.7. Output of EL timing error detector is given by

$$x = \text{Re} \left\{ a_n^* \tilde{\alpha}_n^* \sum_{k=nN_c}^{(n+1)N_c-1} \left(r \left(kT_c + \frac{T_c}{2} + \hat{\tau} \right) - r \left(kT_c - \frac{T_c}{2} + \hat{\tau} \right) \right) c_k \right\} \quad (3.12)$$

The timing error detector (TED) operates on two classes of samples of the matched filter output: one taken early and one taken late with respect to the detection path as shown in Figure 3.8. For a good compromise between implementation complexity and performance, the early and late branches are usually spaced half a chip apart ($T_c/2$) from the detection branch. In the case of no timing error, everything is apparently balanced, hence resulting on average in no signal at the output of the timing error detector at all. In the case where the signal is delayed by $T_c/2$, the late branch is perfectly aligned and therefore delivers a large positive output. The output of the overall timing error detector is calculated as the difference between late and early branch outputs. In the aforementioned case, this causes a

positive value at the TED output while the input signal with positive delays. In the case of negative delays with respect to the receiver time base, the output becomes negative.

If we assume a flat fading channel ($L=1$) case with normalized channel coefficient ($|\tilde{\alpha}|^2 = 1$), the mean output of the timing error detector is

$$E[x] = \text{Re} \left\{ E[|a|^2] |\tilde{\alpha}|^2 \left[R_g \left(T_c/2 + \hat{\tau} - \tau \right) - R_g \left(-T_c/2 + \hat{\tau} - \tau \right) \right] \right\} \quad (3.13)$$

If the environment is multipath fading channel, the mean output of the timing error detector will become

$$\begin{aligned} E[x] &= E[|\tilde{a}|^2] \text{Re} \left\{ \tilde{\alpha}_m^* \sum_{l=0}^{L-1} \tilde{\alpha}_l \left[R_g \left(T_c/2 + \hat{\tau} - \tau \right) - R_g \left(-T_c/2 + \hat{\tau} - \tau \right) \right] \right\} \\ &= E[|a|^2] \text{Re} \left\{ |\tilde{\alpha}_m|^2 \left[R_g \left(T_c/2 + \hat{\tau}_m - \tau_m \right) - R_g \left(-T_c/2 + \hat{\tau}_m - \tau_m \right) \right] \right\} \quad (3.14) \\ &+ E[|a|^2] \text{Re} \left\{ \underbrace{\tilde{\alpha}_m^* \sum_{\substack{l=0 \\ l \neq m}}^{l=L} \tilde{\alpha}_l \left[R_g \left(T_c/2 + \hat{\tau}_m - \tau_l \right) - R_g \left(-T_c/2 + \hat{\tau}_m - \tau_l \right) \right]}_{\text{multipath interference terms}} \right\} \end{aligned}$$

The multipath interference terms will cause error to the output of timing error detector. Especially when the multipath is closely to the desired path as illustrated in Figure 3.9, the accuracy of the TED will be affected deeply. Unfortunately, one important characteristic of indoor UWB channel is dense multipaths due to the extreme high bandwidth which can resolve several multipath components. Therefore a new code tracking scheme should be provided to cancel the multipath interference. According to [26], it is achievable to calculate the fading coefficients and relative delays of the multipath interference, hence the interference terms are possible to be canceled. The new code tracking loop with multipath cancellation scheme is shown in Figure 3.10, after the multipath interference being canceled, the timing error signal will be given by

$$\tilde{x}_m = x_m - \text{Re} \left\{ \hat{\alpha}_m^* \sum_{l=0, l \neq m}^{L-1} \hat{\alpha}_l S(\hat{\tau}_l - \hat{\tau}_m) \right\} \quad (3.15)$$

where $S(\hat{\tau}_l - \hat{\tau}_m)$ is the multipath interference to m th (desired) path caused by the l th path. The scheme is not limited by any assumptions made on the minimum spacing of paths. Therefore, it is able to track closely spaced paths well to and below one chip apart. The paths are tracked individually and the tracker will follow each of them correctly if they eventually diverge again. This technique proposed in [26] is not limited by the fact that it has to focus to the stronger paths, as often supposed in heuristic solutions for dealing with this type of scenarios. But under indoor UWB environment, the closed multipaths are rich; this will cause the cancellation mechanism to be too complex. Hence we propose a new multipath interference cancellation scheme computes neighboring interference only. As shown in Figure 3.9, the interference can be calculated by the peak value of the neighboring with a scale. The scale value can be obtained due to the known transmitted pulse waveform. Hence the proposed code tracking loop with multipath cancellation scheme shown in Figure 3.11 is less complex compared with the technique proposed in [26].

3.2.3 Automatic Frequency Control Loop

Because of the mismatch of the RF component between transmitter and receiver, the received signal will suffer phase rotation caused by the frequency offset. The received signal at baseband after sampling which is given by

$$r_n = s_n e^{-j2\pi\Delta f n T_s} \quad (3.16)$$


where s_n is the transmitted signal, Δf is the difference between the transmitter and

receiver carrier frequencies, T_s is the sampling period. In DS-UWB system, the proposed preamble can help receiver to use efficient maximum likelihood algorithm to estimate and correct for the frequency offset, before the actual information portion of the packet starts.

The proposed automatic frequency control loop [27] which operates on the received is shown in Figure 3.12. The complex conjugate of the received data delayed by NT_s will become

$$r_{n+N}^* = s_{n+N} e^{j2\pi\Delta f(n+N)T_s} \quad (3.17)$$

and the complex product of r_n and r_{n+N}^* after summation is given by

$$\begin{aligned} z &= \sum_{n=0}^{L-1} s_n e^{-j2\pi\Delta f n T_s} \cdot s_{n+N}^* e^{j2\pi\Delta f(n+N)T_s} \\ &= \sum_{n=0}^{L-1} s_n s_{n+N}^* e^{-j2\pi\Delta f n T_s} e^{j2\pi\Delta f(n+N)T_s} \\ &= e^{j2\pi\Delta f N T_s} \sum_{n=0}^{L-1} |s_n|^2 \end{aligned} \quad (3.18)$$


This gives an angle proportional to the frequency offset, and the frequency offset estimator is formed as

$$\hat{f}_\Delta = \frac{1}{2\pi N T_s} \angle z \quad (3.19)$$

3.3 Channel Equalization for IEEE 802.15.3a DS-UWB System

For reliable communication system performance in frequency-selective channels, the channel-induced ISI must be mitigated; channel equalization is an important block to compensate the effect in receiver. Though blind methods have

received a great deal of research attention their initial data detection errors will inhibit adoption, especially in burst-mode systems. Therefore, block-oriented approaches that use preamble sequence are more reliable. In this section, we present a complete equalization technique for IEEE802.15.3a DS-UWB system to compensate the channel effect.

Wireless communication systems require signal processing techniques that improve the link performance. Equalization is one of the most common techniques to compensate for ISI created by multipath channel. In IEEE 802.15.3a DS-UWB system, it is suggested that receiver with decision feedback equalizer (DFE) can support good ability to mitigate ISI effect.

The basic idea of DFE is that once an information symbol has been detected and decided upon, the ISI that it induces on future symbols can be estimated and subtracted out before detection of subsequent symbols. The DFE can be realized in a direct transversal form as shown in Figure 3.13. It consists of a feed forward filter (FFF) and a feed back filter (FBF). The FFF can deal with precursor and postcursor ISI and FBF can perfectly cancel postcursor ISI.

The minimum mean square error (MMSE) is a robust algorithm which the tap weights are chosen to minimize the MSE of all the ISI terms plus the noise power at the output of the equalizer [17].

$$\mathbf{q}_f, \mathbf{q}_b = \arg \min E \left\{ s(t) - \mathbf{q}_f \mathbf{r}_c(t) + \mathbf{q}_b \hat{s}(t) \right\} \quad (3.20)$$

where $\mathbf{q}_f = \left\{ q_{f_0}, q_{f_1}, \dots, q_{f_{K_f-1}} \right\}$ is the tap weights of the FFF, $\mathbf{q}_b = \left\{ q_{b_0}, q_{b_1}, \dots, q_{b_{K_b-1}} \right\}$ is the tap weights of the FBF, $\mathbf{r}_c(t)$ is the received data, and $\hat{s}(t)$ is the output after the slicer.

Ideally, the number of equalizer taps should be enough to cover the delay spread

of the channel. But the channel length under UWB environment is extreme long due to the ultra short pulse. To design the equalizer with sufficient taps number is inefficient. Fortunately, the paths with dominating power are usually gathered closely instead of uniformly distributed. Hence the length of equalizer is designed to cover a particular part of the channel length can gather most of the multipath energy. In this thesis, we choose the length of equalizer to cover each path that excess -10 dB compared to the strongest path by the channel PDP. The PDP of CM1 and CM2 is shown in Figure 3.14(a), and that of CM3 and CM4 is shown in Figure 3.14(b). By these, we can distinctly define the system parameter for each channel.

3.4 Computer Simulations

Computer simulations are conducted to evaluate the performance of bit error rate (BER) and packet error rate (PER) in the IEEE 802.15.3a DS-UWB system. In the simulation, the relationship between SNR and E_b/N_0 can be defined as

$$SNR = \frac{P_{signal}}{P_{noise}} = \frac{E_b \times R_b}{N_0 \times B} = \frac{E_b \times R_b}{N_0 \times (N_c R_b)} = \frac{1}{N_c} \frac{E_b}{N_0} \quad (3.21)$$

where P_{signal} is the signal power, P_{noise} is the noise power, E_b is the bit energy, R_b is the bit rate, B is the bandwidth of the chip sequence, and N_c is the processing gain. When the system transmit power is normalized to one, the noise power given by σ^2 corresponding to a specific E_b/N_0 can be generated by

$$\sigma^2 = \frac{N_0}{E_b} \quad (3.22)$$

The numbers of equalizer tap for different situations (CM1 to CM4) are listed in Table 3.2. In the following simulations, we choose the mandatory BPSK modulation

mode operating in the low band and the best 90 out of 100 channel realizations. All of the system parameters are estimated by the algorithms mentioned in Sections 3.2 and 3.3. In the first simulation, we evaluate the DS-UWB system performance with 110 Mbps data rate. The BER and PER performances as a function of input SNR E_b/N_0 are shown in Figures 3.15 and 3.16 respectively. It is observed that with sufficient equalizer taps, the BER and PER system performances decrease as E_b/N_0 increase. Besides, under longer range environments like CM3 and CM4, the system performances are a little worse than that in shorter range environments due to the inaccuracy of system parameter estimation. Next, the BER and PER performances with 220 Mbps data rate are shown in Figures 3.17 and 3.18 respectively. Compared with the 110 Mbps mode, both BER and PER performances are worse due to the shorter spreading code length which will induce more serious ISI. Finally, BER and PER performances with 500 Mbps data rate are shown in Figures 3.19 and 3.20 respectively. The shorter spreading code length and higher code rate lead the system performances to be worse compared with the previous modes.

3.5 Summary

In this chapter, we first introduce the S-V model which is used to form indoor UWB channel environment. Compared with conventional narrowband channel models, the clustering phenomenon is observed in the channel. Furthermore, the dense and long delay spread multipaths will lead some receiver function blocks to be modified. All the receiver function block algorithms have been described in Sections 3.2 and 3.3. The channel characteristic of dense multipaths will cause the conventional EL code-tracking loop to fail and the proposed EL code-tracking loop with multipath cancellation scheme can effectively overcome this problem. Besides,

the channel length is different under different situations (CM1 to CM4), and we have defined different numbers of equalizer tap in Section 3.3. The performance of all algorithms mentioned in this chapter has been evaluated by Matlab. Computer simulations show that the proposed algorithms work as expected.



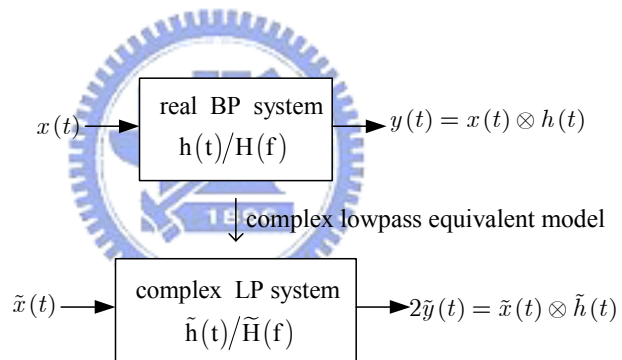
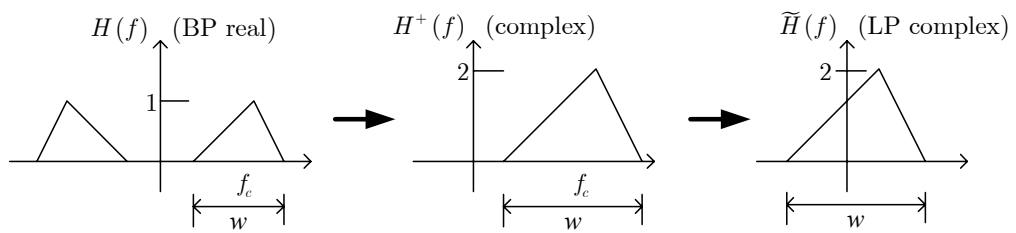


Figure 3.1 Simulation of passband system in terms of equivalent complex baseband system

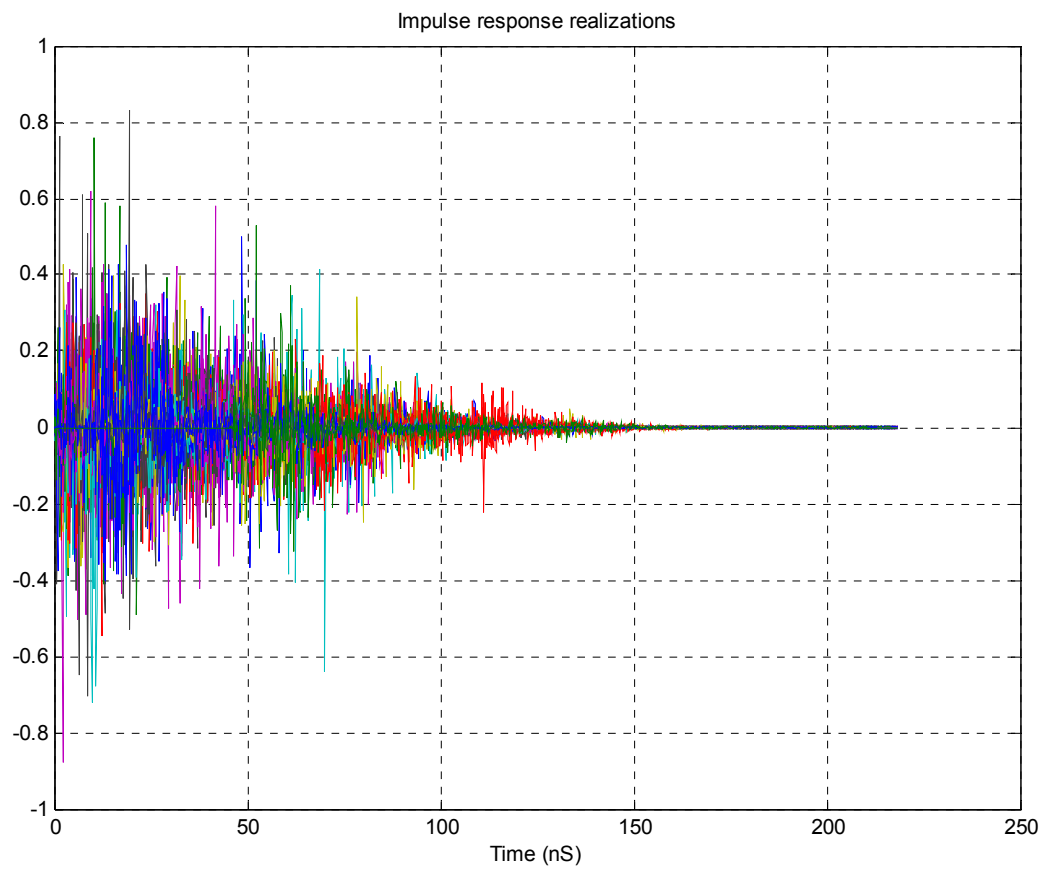


Figure 3.2 Superposition of 100 impulse responses based on the CM3 channel model (NLOS up to 10 m with average RMS delay spread of 15 ns).

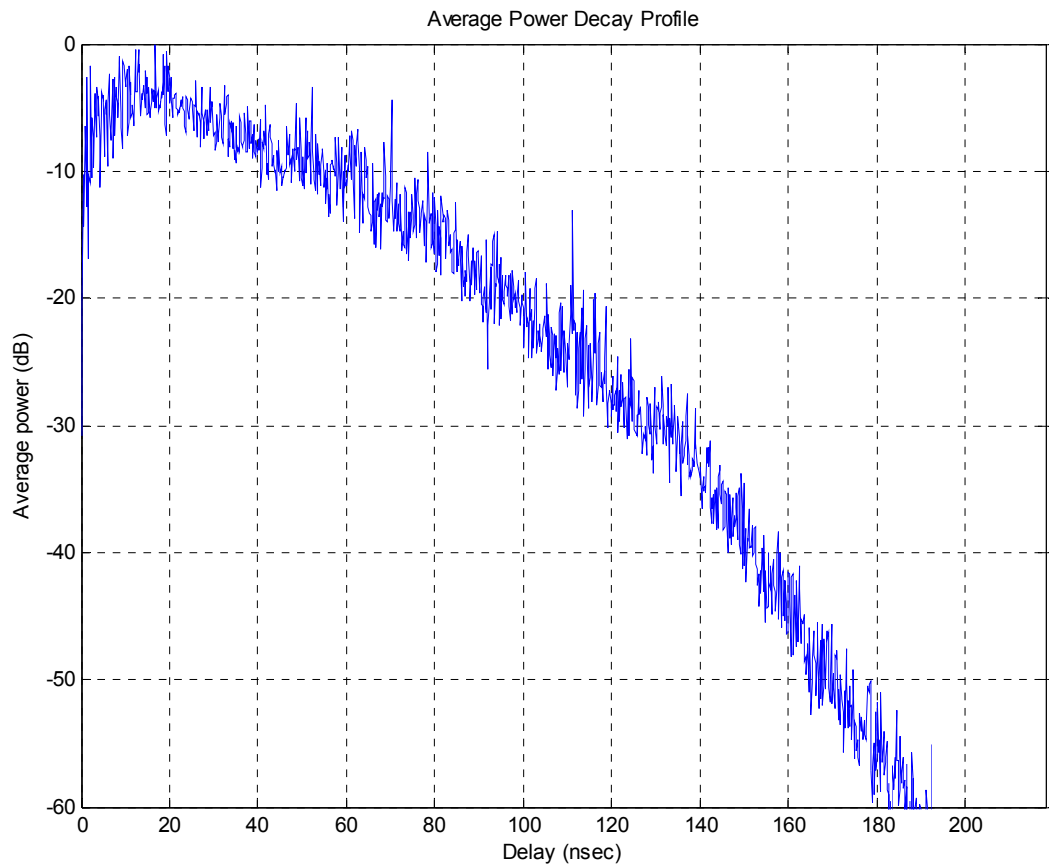


Figure 3.3 Average power decay profile for the channel model CM3 (NLOS up to 10 m with average RMS delay spread of 15 ns).

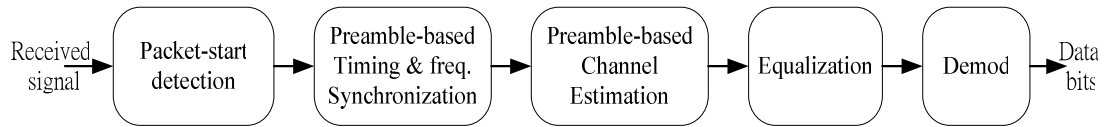


Figure 3.4 IEEE 802.15.3a DS-UWB receiver working flow

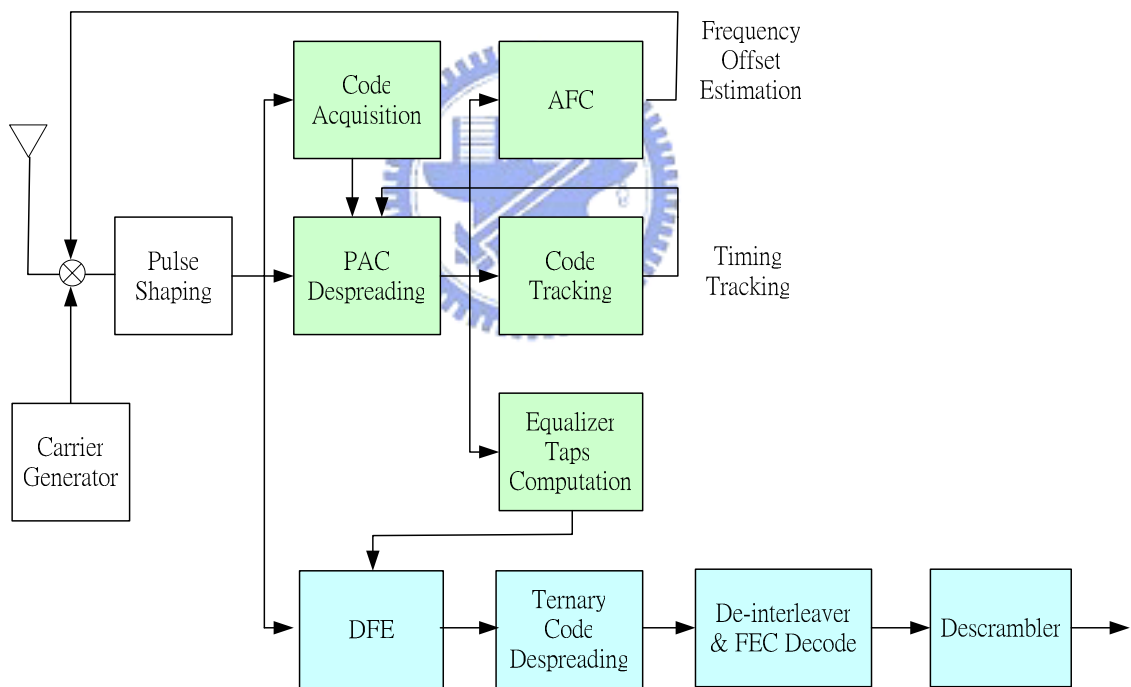


Figure 3.5 Proposed receiver architecture of IEEE 802.15.3a DS-UWB system

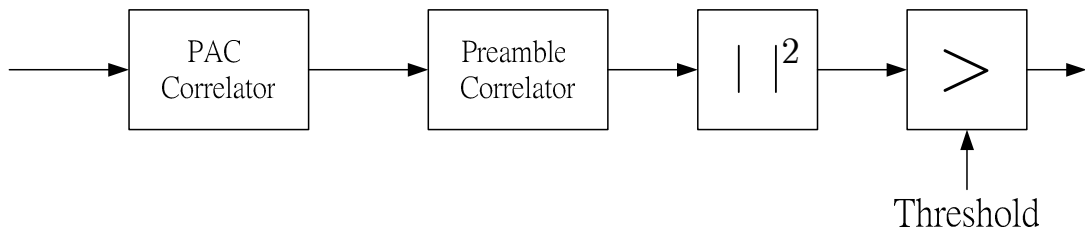


Figure 3.6 Code acquisition structure of IEEE 802.15.3a DS-UWB system

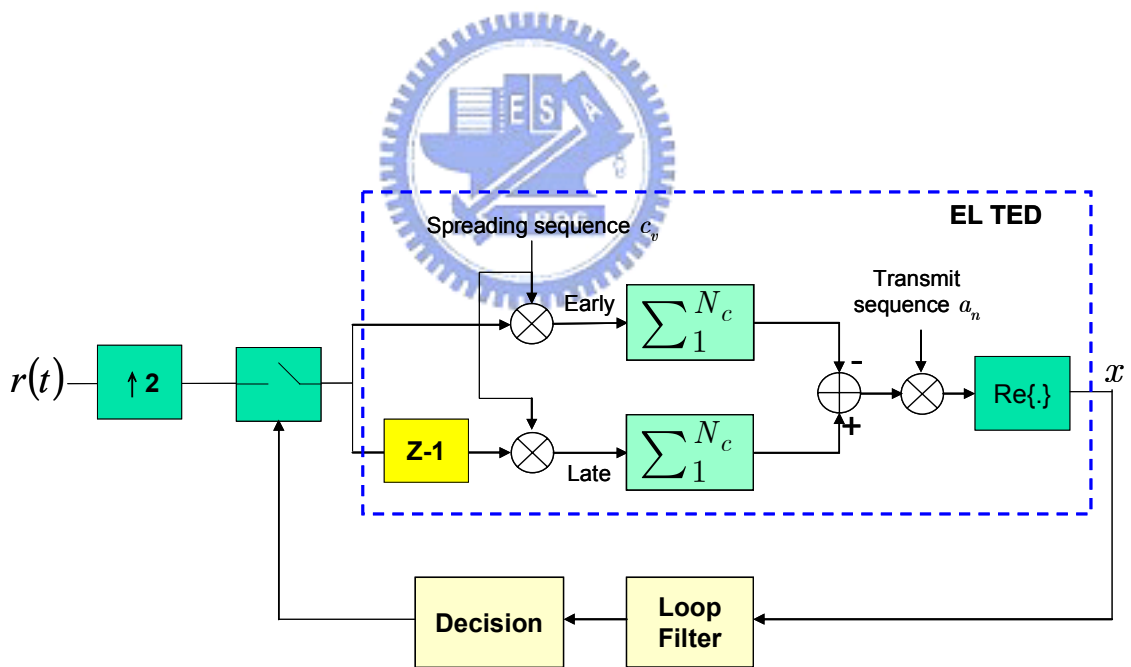


Figure 3.7 Conventional early-late code tracking loop architecture

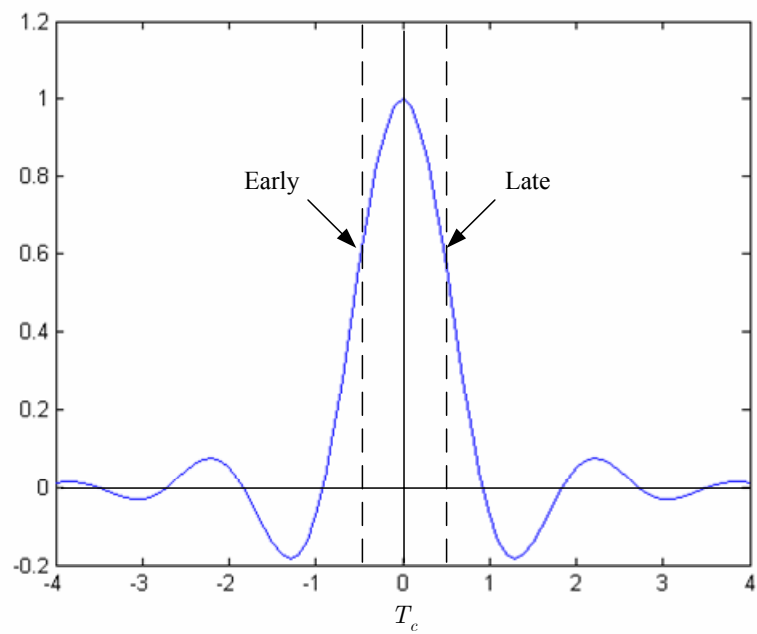


Figure 3.8 Comparison between early and late edges for the detecting path

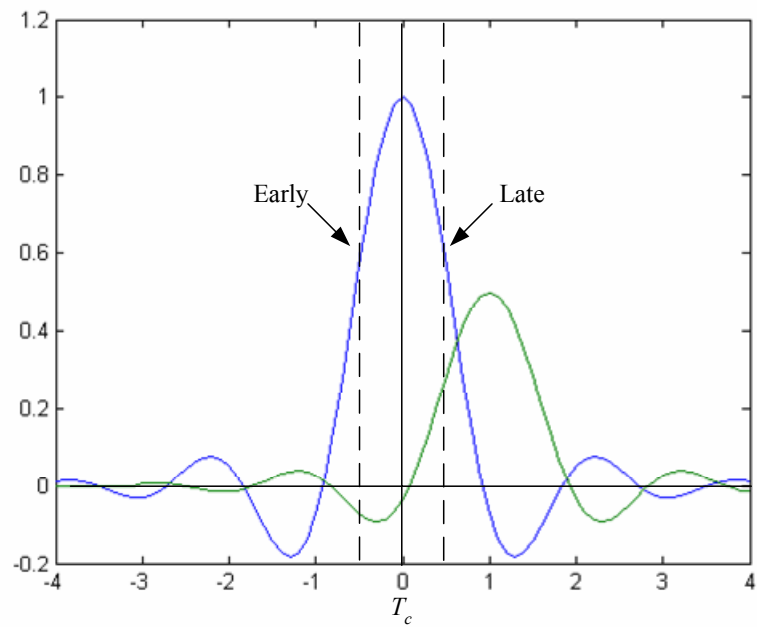


Figure 3.9 Comparison between early and late edges under dense multipaths environment

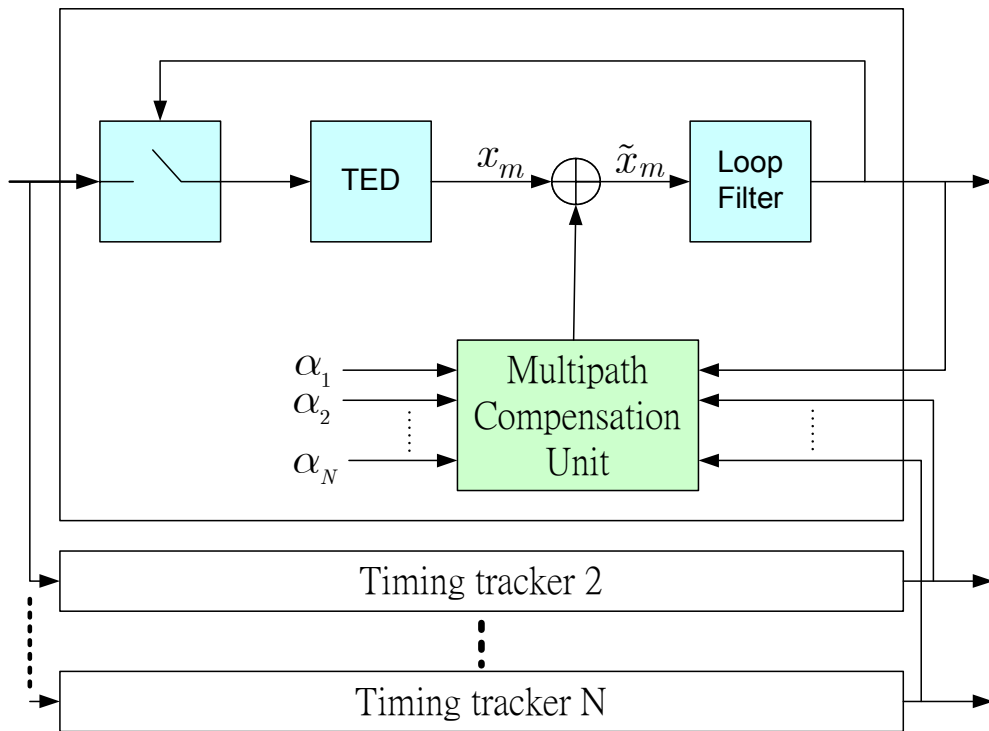


Figure 3.10 Structure of cancellation mechanism for IEEE 802.15.3a DS-UWB system

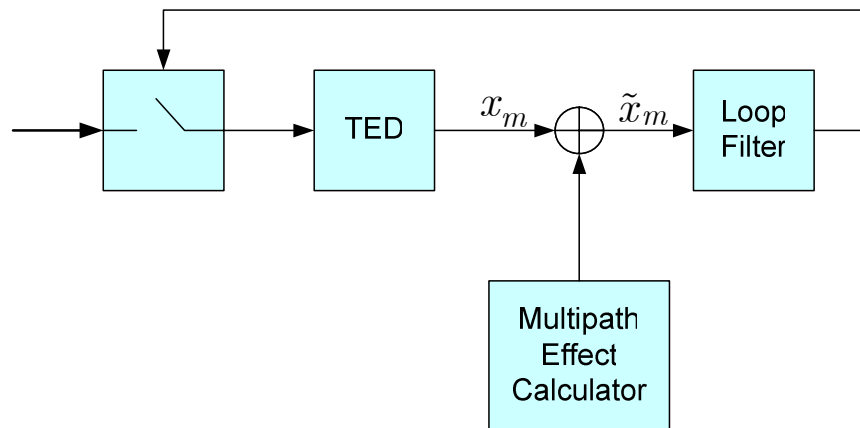


Figure 3.11 Proposed code tracking loop with multipath cancellation scheme for IEEE 802.15.3a DS-UWB system

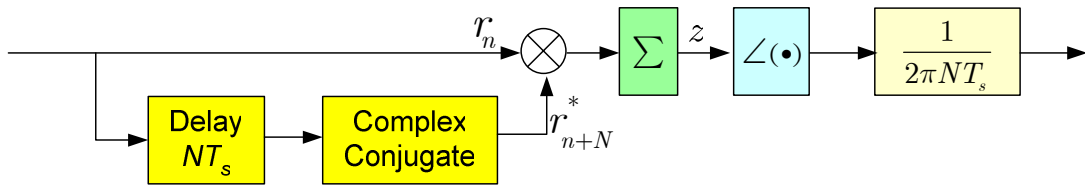


Figure 3.12 Proposed automatic frequency control loop architecture for IEEE 802.15.3a DS-UWB system

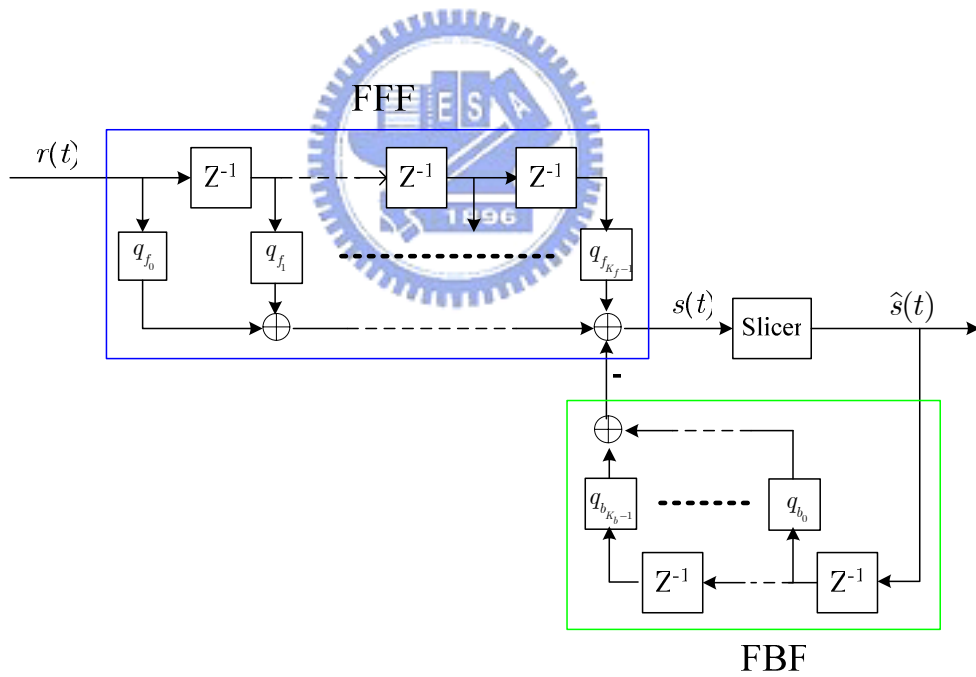
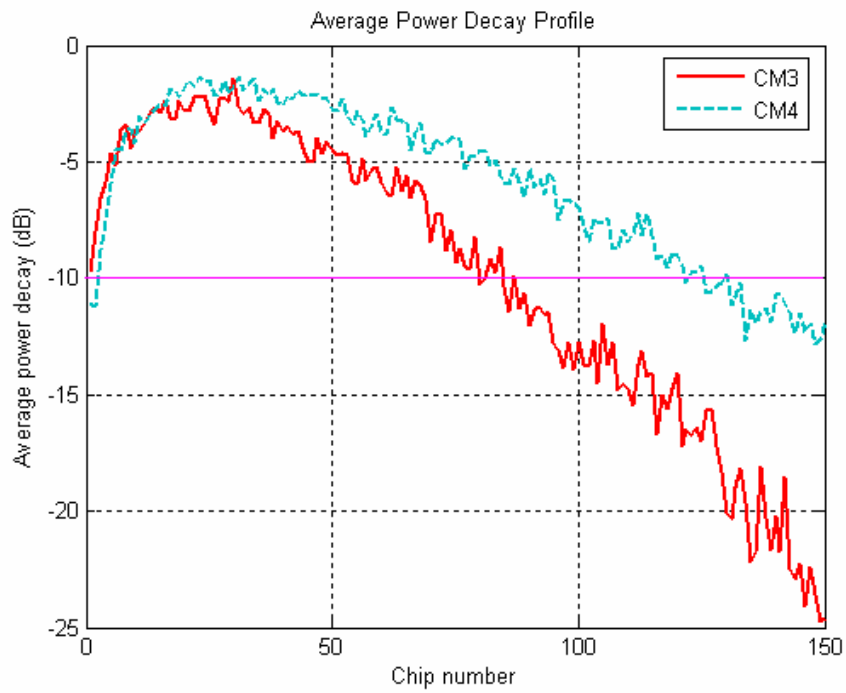
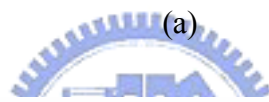
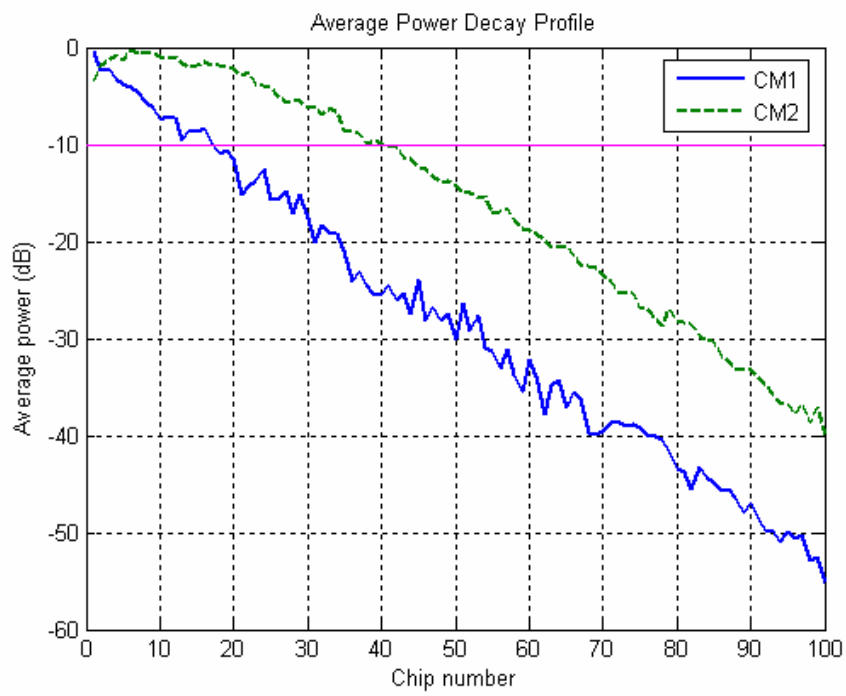


Figure 3.13 Decision feedback equalizer architecture



(b)

Figure 3.14 Average power decay profile for different situations (a) CM1 and CM2 (b) CM3 and CM4

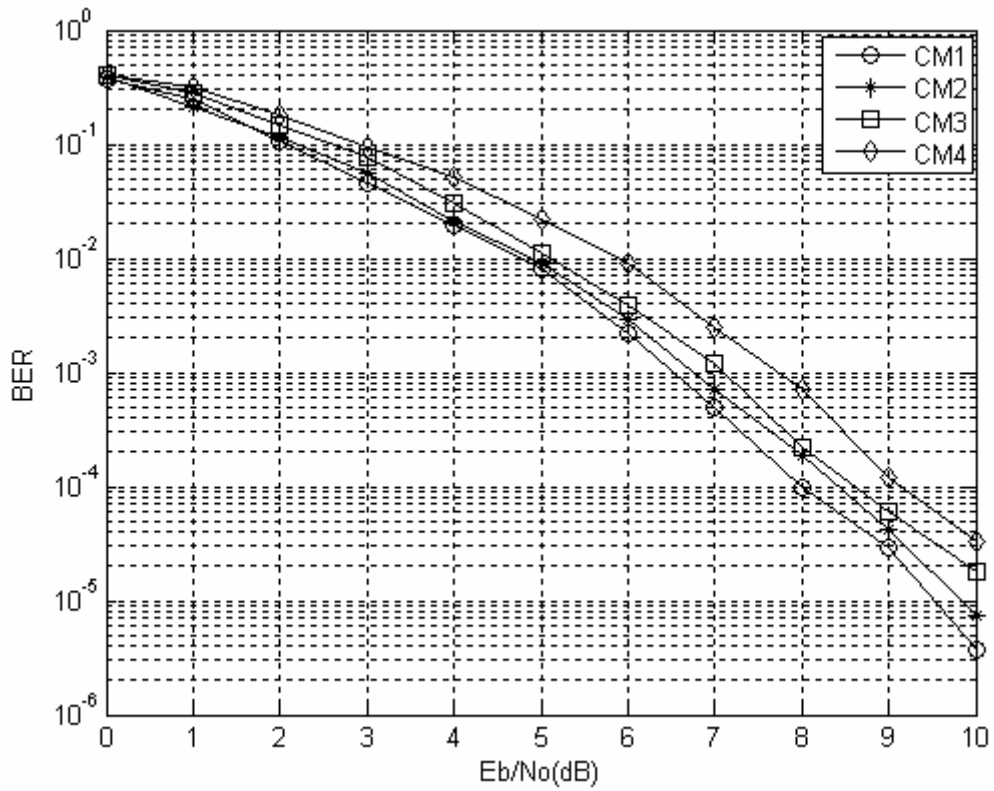


Figure 3.15 BER performances of DS-UWB system with 110 Mbps data rate under different environments (CM1 to CM4)

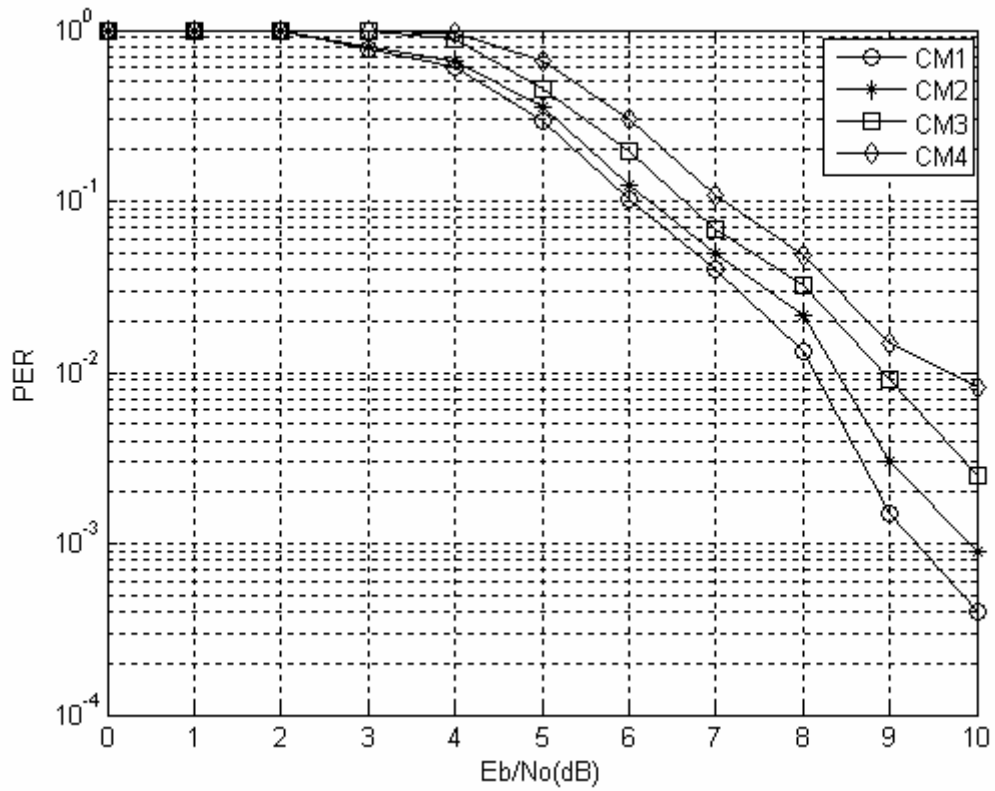


Figure 3.16 PER performances of DS-UWB system with 110 Mbps data rate under different environments (CM1 to CM4)

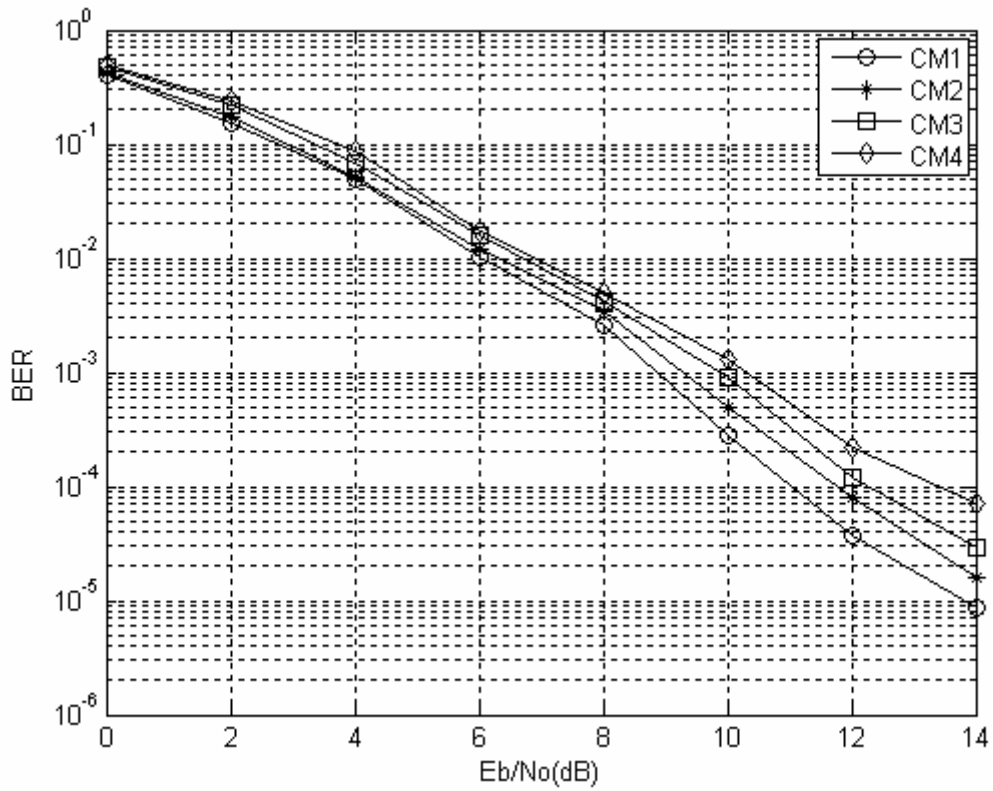


Figure 3.17 BER performances of DS-UWB system with 220 Mbps data rate under different environments (CM1 to CM4)

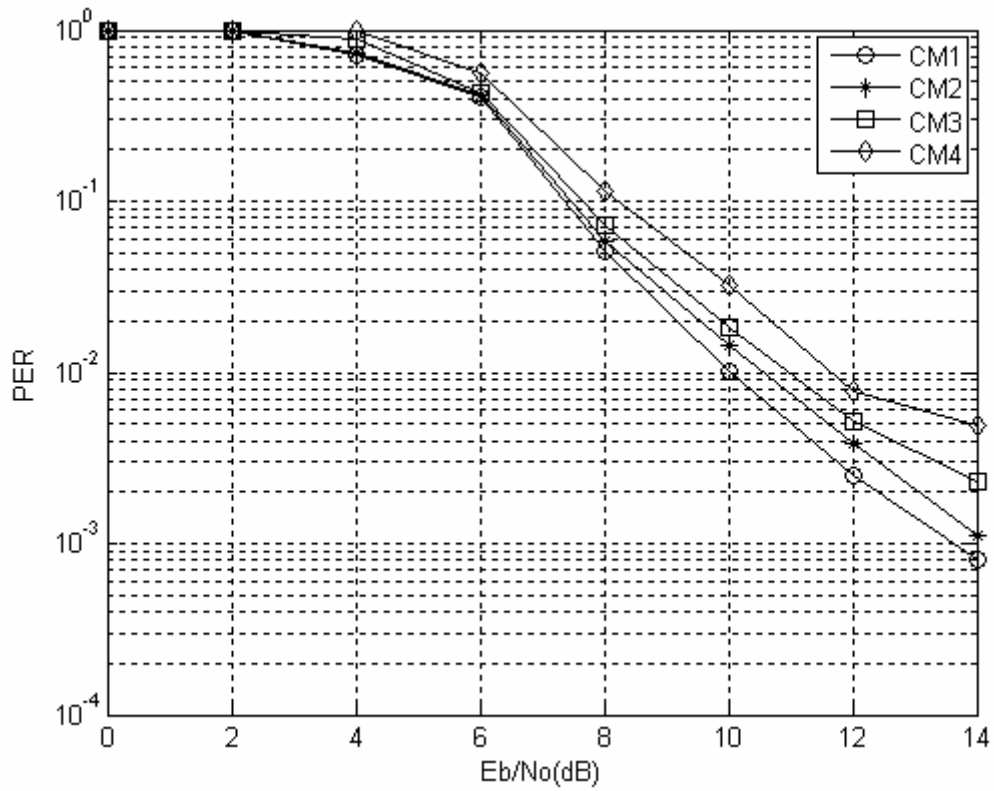


Figure 3.18 PER performances of DS-UWB system with 220 Mbps data rate under different environments (CM1 to CM4)

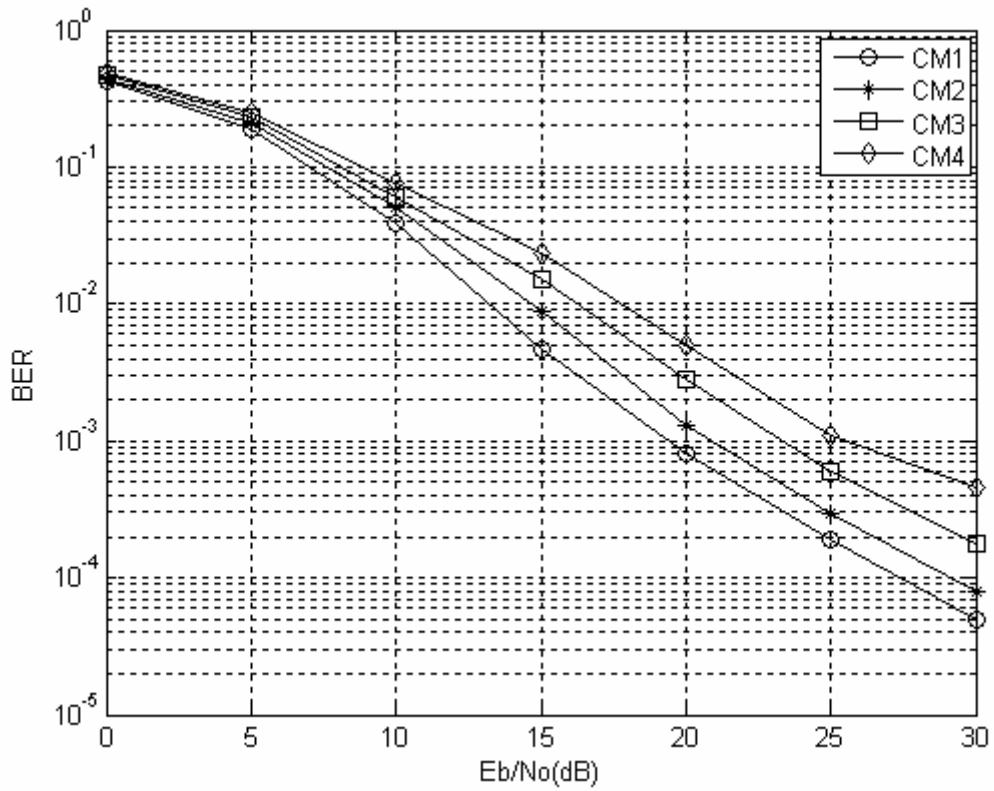


Figure 3.19 BER performances of DS-UWB system with 500 Mbps data rate under different environments (CM1 to CM4)

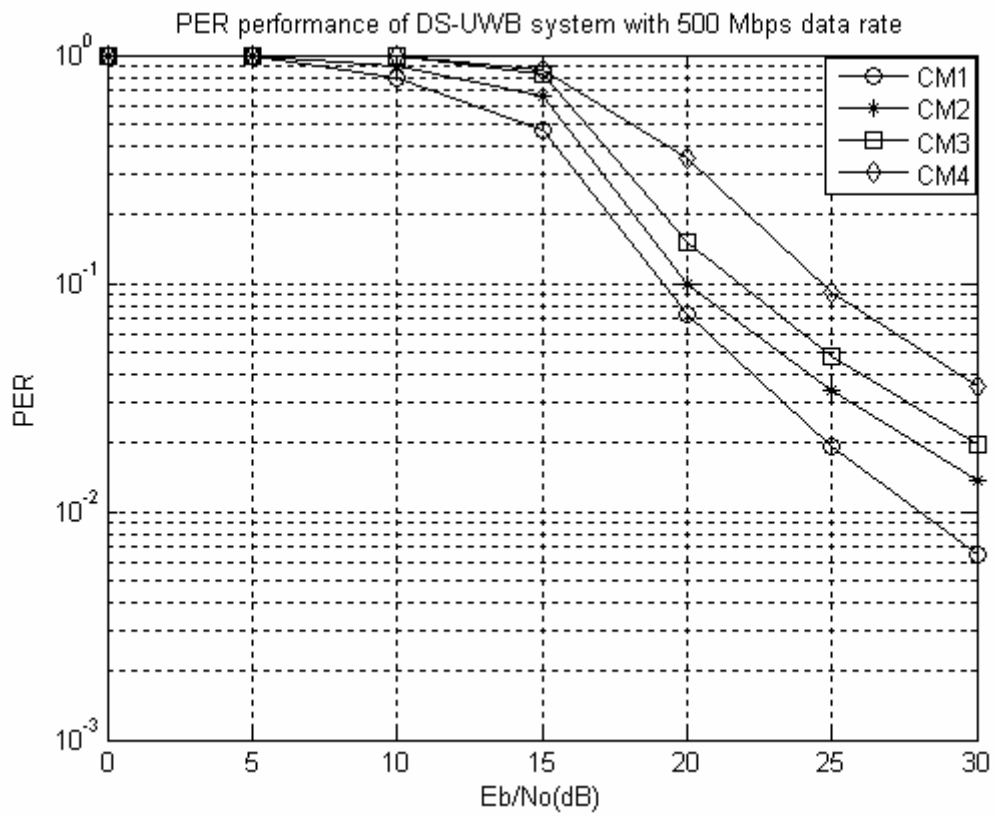


Figure 3.20 PER performance of DS-UWB system with 500 Mbps data rate under different environments (CM1 to CM4)

Table 3.1 Multipath channel target characteristics and model parameters

Target Channel Characteristics	CM 1	CM 2	CM 3	CM 4
Mean excess delay (nsec) (τ_m)	5.05	10.38	14.18	
RMS delay (nsec) (τ_{rms})	5.28	8.03	14.28	25
NP _{10dB}			35	
NP (85%)	24	36.1	61.54	
Model Parameters				
Λ (1/nsec)	0.0233	0.4	0.0667	0.0667
λ (1/nsec)	2.5	0.5	2.1	2.1
Γ	7.1	5.5	14.00	24.00
γ	4.3	6.7	7.9	12
σ_1 (dB)	3.3941	3.3941	3.3941	3.3941
σ_2 (dB)	3.3941	3.3941	3.3941	3.3941
σ_x (dB)	3	3	3	3
Model Characteristics				
Mean excess delay (nsec) (τ_m)	5.0	9.9	15.9	30.1
RMS delay (nsec) (τ_{rms})	5	8	15	25
NP _{10dB}	12.5	15.3	24.9	41.2
NP (85%)	20.8	33.9	64.7	123.3
Channel energy mean (dB)	-0.4	-0.5	0.0	0.3
Channel energy std (dB)	2.9	3.1	3.1	2.7

Table 3.2 Equalizer tap numbers for different environments

	CM 1	CM 2	CM 3	CM 4
FFF	18	40	80	120
FBF	9	20	40	60

Chapter 4

Pre-Rake Diversity Combining Technique for IEEE 802.15.3a DS-UWB System

Because of the long delay spread characteristic of UWB channel, the receiver needs an equalizer with large number taps to overcome the multipath ISI effect. This leads the complexity of receiver to increase. Hence, we will use the Pre-Rake diversity combining technique into IEEE 802.15.3a DS-UWB system to reduce the receiver complexity. The rest of this chapter is organized as follows. Pre-Rake diversity combining concepts will be introduced in Section 4.1. According to the UWB environment, we propose Selective-Pre-Rake diversity combining using the channel information on the L strongest paths in Section 4.2. Channel estimation algorithms will be developed in Section 4.3. Although the Pre-Rake diversity combining technique is adopted to effectively capture multipath energy, we propose a simplified equalizer at receiver to improve system performance in Section 4.4. Finally, we evaluate the proposed system in Section 4.5.

4.1 Pre-Rake Diversity Combining for DSSS Communications Systems

In a wireless communication environment, the combination of the received signals from diverse independent paths or mediums can improve the system performance. For systems operating in a multipath environment, signals of any two paths with a propagation delay difference of more than the chip duration T_c are separated at the output of the matched filter as two distinct peaks. These peaks which represent the signal strength from each path can be combined to reduce the fading effects of the channel.

4.1.1 Diversity Combining Methods

The diversity combining methods directly applicable to the DS-SS communications are as follows [28]:

1. **Selection combining:** in this method the signal from the path with the highest power is selected and the remaining signals are discarded. For example, if path i has the highest received power, the weighing factor w_i is set to one (or generally to a constant) and all the other w_k are set to zero.
2. **Maximum ratio combining:** in this method the phase locked signals from each path are added together in a way that the more powerful signals are emphasized and the less reliable ones are suppressed. In other words the factors w_k are related to the individual path strength. For a Maximum Ratio combiner the BER can be calculated from [28]

$$P_{mr} = \frac{1}{2} \prod_{i=1}^L \left(\frac{1}{1 + \Gamma_i} \right) \quad (4.1)$$

where is the average SNR of the i th path.

3. **Equal gain combing:** where the phase locked output of path diverse signals are combined equally with all weighing factors a_k set to a constant. This method is inferior than the Rake method by only about 1.3 dB when the number of diversity paths is more than 3 [29].

4.1.2 Rake Combining Scheme

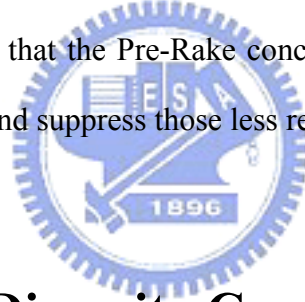
The Rake combining is a form of the maximum ratio combining method in DSSS communications. The only difference is that tap settings for a_k factors are carried out in intervals and not continuously as it would be done in an ideal maximum ratio combiner. A Rake diversity combiner is shown in Figure 4.1. The input signal is $s(t)$. The filter is matched to $s(t)$ and its output would be equal to the input of the spreader if noise and multipaths did not exist. Hence, the signal at the output of the matched filter can be written as sum of the signals from L different paths

$$r(t) = \sum_{i=0}^{L-1} \tilde{\alpha}_i s(t - \tau_i) + n(t) \quad (4.2)$$

The optimum weighting factors of Figure 4.1 can be derived for the Rake combining diversity method to be proportional to the individual path strengths [29]. And the Rake combining concept is shown in Figure 4.2.

4.1.3 Pre-Rake Combining Scheme

The Pre-Rake combining is to move the diversity combiner to the transmitter [30], and the block diagram is shown in Figure 4.3. The Pre-Rake combining concept is shown in Figure 4.4. The Rake signal was seen to be a combining of the multipath signals. If the strength and the corresponding relative phase of a path can be measured for the present data burst and estimated for the near future, a number of future transmissions can be arranged so the received signal has the characteristic of a Rake diversity signal. Each one of these transmissions is delayed according to the estimated relative path delay, and amplified according to the estimated path strength and relative path phase. This is almost an identical operation to the one performed in a Rake receiver, the only difference being that this time the operation is done in the transmitter. It could be said that the Pre-Rake concept is to accentuate transmission for the more reliable paths and suppress those less reliable.



4.2 Pre-Rake Diversity Combining for IEEE 802.15.3a DS-UWB System

The structure of Pre-Rake system has been shown in Section 4.1. The transmitted signal as the form in (3.9) with data sequence $d_n \in \{+1, -1\}$ and spreading code $\{c_n\}$ defined in Table 2.2 and 2.3 can be given by

$$s(t) = \sum_n d_n \sum_{v=0}^{N_c-1} c_v g(t - vT_c) \quad (4.3)$$

and the Pre-Rake combiner (PRC) which is defined by the time-reversal and conjugation of the channel response [31] defined in (3.7) is given by

$$h_t(t) = \sum_{i=0}^{L-1} \tilde{\alpha}_{L-i}^* \delta(t - \tau_i) \quad (4.4)$$

The received signal can be rewritten by

$$r_1(t) = s(t) * h_t(t) * h(t) + n(t) \quad (4.5)$$

hence we can split the received symbol into the part containing desired symbol and the other one for the ISI which can be given by

$$r_1(k) = \underbrace{\sum_{l=0}^{L-1} |\tilde{\alpha}_l \tilde{\alpha}_l^*| s(k)}_{\text{desired part}} + \underbrace{\sum_{k \neq 0} \sum_{m \neq l} \tilde{\alpha}_l \tilde{\alpha}_m^* \delta(k - l - m) s(n - k)}_{\text{ISI terms}} + n(k) \quad (4.6)$$

Assume the transmit signal power is P_{signal} and AWGN noise power is σ^2 . The power of received symbol can be expressed as

$$E[|r_1(k)|^2] = P_{\text{signal}} E[P_D] + P_{\text{signal}} E[P_{\text{ISI}}] + \sigma^2 \quad (4.7)$$

The constant P_D and P_{ISI} are the instant useful power and the ISI power, respectively,

$$P_D = \left| \sum_{l=0}^{L-1} \tilde{\alpha}_l \tilde{\alpha}_l^* \right|^2 \quad (4.8)$$

$$P_{\text{ISI}} = \left| \sum_{k \neq 0} \sum_{m \neq l} \tilde{\alpha}_l \tilde{\alpha}_m^* \delta(k - l - m) \right|^2 \quad (4.9)$$

We can now define the effective SNR as

$$\text{SNR}_{\text{eff}} = \frac{P_{\text{signal}} E[P_D]}{P_{\text{signal}} E[P_{\text{ISI}}] + \sigma^2} = \frac{E[P_D]}{E[P_{\text{ISI}}] + \frac{1}{\rho_0}} \quad (4.10)$$

where $\rho_0 = \frac{P_{\text{signal}}}{\sigma^2}$ is the SNR under AWGN channel.

However, it is impossible to combine all multipath under UWB channel due to the extreme large number of multipaths. Hence, the Selective-Pre-Rake (S-Pre-Rake) diversity combining proposed in [32] will be a suitable technique for DS-UWB system to combine multipath energy effectively.

The concept of S-Pre-Rake is shown in Figure 4.5. The system selects only the strongest P paths to combine energy. The equivalent channel $\mathbf{h}'_p = \mathbf{h}'_t * \mathbf{h}$ at receiver is still similar to a single path channel. Next, we need to define the Rake finger number for different situation by the equivalent channel \mathbf{h}'_p . The system parameters are selected by the ratio of desired path power to ISI path power $\frac{P_D}{P_{ISI}}$, the result is shown in Figure 4.6. Hence the S-Pre-Rake finger number can be defined in Table 4.1.



4.3 Channel Estimation for IEEE 802.15.3a DS-UWB System

In order to achieve S-Pre-Rake technique, the channel impulse response must be estimated first. Though blind methods have received a great deal of research attention their initial data detection errors will inhibit adoption, especially in burst-mode systems. Therefore, block-oriented approaches that use preamble sequence estimation are more reliable.

4.3.1 Channel Estimation via Correlation

The transmitted and received signal as mentioned in (3.9) and (3.10), here we use the matrix form $\mathbf{h} = [\tilde{\alpha}_0, \tilde{\alpha}_1, \dots, \tilde{\alpha}_{L-1}]^T$ to represent proposed S-V model channel. And the transmitted preamble spread by the PAC is denoted by $\mathbf{s} = [s_0, s_1, \dots, s_{N_c-1}]^T$, so that the received signal $\mathbf{r} = [r_0, r_1, \dots, r_{L+N_c-2}]^T$ is given by

$$\mathbf{r} = \mathbf{S}\mathbf{h} + \mathbf{w} \quad (4.11)$$

where \mathbf{S} is the Toeplitz $(L+N_c-1) \times L$ matrix which is represented by

$$\mathbf{S} = \begin{bmatrix} s_0 & 0 & 0 & \cdots & 0 \\ s_1 & s_0 & 0 & \ddots & 0 \\ \vdots & s_1 & s_0 & \ddots & \vdots \\ s_{N_c-1} & \vdots & s_1 & \ddots & 0 \\ 0 & s_{N_c-1} & \vdots & \ddots & s_0 \\ 0 & 0 & s_{N_c-1} & \ddots & s_1 \\ \vdots & \vdots & \vdots & \ddots & \vdots \\ 0 & 0 & 0 & \cdots & s_{N_c-1} \end{bmatrix} \quad (4.12)$$

and $\mathbf{w} = [w_0, w_1, \dots, w_{N_c-1}]^T$ is additive white Gaussian noise

The correlation is performed between the received signal and a copy of the transmitted sequence to obtain the estimated channel $\tilde{\mathbf{h}} = [\hat{\alpha}_0, \hat{\alpha}_1, \dots, \hat{\alpha}_{L-1}]^T$ given by

$$\tilde{\alpha}_k = \frac{1}{N_c} \sum_{n=k}^{N_c-1+k} r_n \cdot s_{n-k} \quad \text{or} \quad \tilde{\mathbf{h}} = \frac{1}{N_c} \mathbf{S}^T \mathbf{r} \quad (4.13)$$

and (4.13) can be rewritten as

$$\tilde{\mathbf{h}} = \mathbf{W}\mathbf{h} + \boldsymbol{\eta} \quad (4.14)$$

where $\boldsymbol{\eta} = \frac{1}{N_c} \mathbf{S}^T \mathbf{w}$ and $\mathbf{W} = \frac{1}{N_c} \mathbf{S}^T \mathbf{S}$ is a symmetric and Toeplitz matrix of autocorrelations which is given by

$$\mathbf{W} = \begin{bmatrix} w_0 & w_1 & \cdots & w_{L-1} \\ w_1 & w_0 & \ddots & \vdots \\ \vdots & w_1 & \ddots & w_1 \\ w_{L-1} & \cdots & w_1 & w_0 \end{bmatrix}_{L \times L} \quad (4.15)$$

and each element is given by

$$w_k = \frac{1}{N} \sum_{m=0}^{N-1-k} s_{m+k} s_m, \quad k = 0, 1, \dots, L-1 \quad (4.16)$$

The optimum correlation-based estimate using this technique would be achieved using a sequence with an ideal thumbtack autocorrelation so that $\frac{1}{N} \mathbf{S}^T \mathbf{S} = \mathbf{W} = \mathbf{I}$

is a diagonal matrix. Hence [33] defined $\mathbf{V} = \mathbf{W} - \mathbf{I}$ is the sidelobe interference matrix.

The j th row (or column) of \mathbf{V} means the interference that corrupts the j th path estimated $\tilde{\alpha}_j$.



4.3.2 Channel Estimation with Sidelobe Cancellation

The estimated interference can be cancelled from all path estimates simultaneously to obtain an improved impulse response estimate $\hat{\mathbf{h}}$ via

$$\begin{aligned} \hat{\mathbf{h}} &= \tilde{\mathbf{h}} - \mathbf{V} \tilde{\mathbf{h}} \\ &= \tilde{\mathbf{h}} - (\mathbf{W} - \mathbf{I}) \tilde{\mathbf{h}} \\ &= \tilde{\mathbf{h}} + \mathbf{W}(\mathbf{h} - \tilde{\mathbf{h}}) + \eta \end{aligned} \quad (4.17)$$

The estimate can be improved by increasing the accuracy of the correlation result $\tilde{\mathbf{h}}$. A sequential computation (SC) presented in [33] can be devised wherein the sidelobe interference contributions are computed for each tentative estimate \tilde{h}_j with the following formula

$$\hat{\mathbf{h}}^{\text{SC}} = \sum_{j=0}^{L-1} \hat{\alpha}_j (\mathbf{e}_{j+1} - \mathbf{v}_j) \quad (4.18)$$

where $\{e_j\}_{j=1}^L$ is the usual standard orthonormal basis for \mathbf{R}^L .

4.4 Simplified Receiver Architecture

In section 4.2, the ability of S-Pre-Rake diversity combining has been proved. Although the S-Pre-Rake diversity combining scheme can form a strong single main path, the rest paths which will induce multipath ISI still can not be eliminated completely. As shown in Figure 4.6, the ratio of desired path power to ISI path power will be saturated between 0 dB and 2 dB. In order to achieve better performance, a simple equalizer at receiver is required can effectively improve system performance. On the other words, the MMSE DFE taps numbers can be decreased significantly.

4.4.1 Post-Cursor Multipath Cancellation

Besides the MMSE DFE mentioned in section 3.3.2. A more simplified post-cursor multipath cancellation (PCMC) scheme proposed in [34] is a less complexity DFE that cancels post-cursor ISI only. As shown in Figure 4.7. Compared to the MMSE DFE, PCMC DFE has only the FBF part. And the tap weights are calculated by the estimated channel $\hat{\mathbf{h}} = [\hat{\alpha}_0, \hat{\alpha}_1, \dots, \hat{\alpha}_{L-1}]$ to cancel all the post secondary paths signal to preserve the main path signal; the output will be given by

$$s(t) = r(t) - \sum_{l=1}^{L-1} \hat{\alpha}_l \hat{s}(t - \hat{\tau}_l) \quad (4.19)$$

where $\hat{s}(t) = \text{slice}[s(t)]$ is the hard decision slicer.

Since the PCMC DFE cancels post-cursor ISI only. Compared with the MMSE DFE, the system performance is a little worse but the complexity is largely decreased

because the inverse matrix computation is unnecessary.

4.5 Computer Simulations

In this section, computer simulations are conducted to evaluate the channel estimation and BER performance of IEEE 802.15.3a DS-UWB systems. In the first simulation, the channel estimation performance of different methods can be measured by comparing the mean square error (MSE)

$$MSE = E \left[(\mathbf{h} - \hat{\mathbf{h}})^T (\mathbf{h} - \hat{\mathbf{h}}) \right] \quad (4.20)$$

whose comparison results for each channel (CM1 to CM4) are shown in Figure 4.8. The techniques with sidelobe cancellation scheme outperform the correlation method as mentioned in Section 4.3.

In the second simulation, we evaluate the BER performances of the DS-UWB system with a joint design of S-Pre-Rake scheme at the transmitter and a simple equalizer at the receiver. In the following simulations, we choose the mandatory BPSK modulation mode operating in the low band the best 90 out of 100 channel realizations. The S-Pre-Rake finger numbers are listed in Table 4.1 and the equalizer tap numbers are listed in Table 4.2. The BER performances of the DS-UWB system of 110 Mbps data rate in CM3 and CM4 by using S-Pre-Rake diversity combining and different equalizer types compared with a high complexity equalizer are shown in Figures 4.9 and 4.10 respectively. It is observed that the performance of using a high complexity equalizer gains 1 to 2 dB for a BER of 10^{-3} compared with the proposed joint design systems. The performances of the simplified MMSE DFE are superior to the PCMC DFE because the MMSE DFE can deal with the pre-cursor ISI

but the PCMC DFE cannot. Next, the BER performances of the DS-UWB system of 220 Mbps data rate in CM3 and CM4 by using S-Pre-Rake diversity combining and different equalizer types compared with a high complexity equalizer are shown in Figures 4.11 and 4.12 respectively. It is observed that the performance of using a high complexity equalizer gains 2 to 4 dB for a BER of 10^{-3} compared with the proposed joint design systems. Compared with the 110 Mbps mode, the shorter spreading code will lead system performance to degrade. Under CM3 environment, the high complexity MMSE DFE needs 80^3+40^2 complex multipliers to compute tap weights. The S-Pre-Rake diversity combining cooperated with simple MMSE DFE system needs only 16^3+16^2 complex multipliers to compute tap weights. The S-Pre-Rake diversity combining cooperated with PCMC DFE system does not need any matrix inversion computation.

4.6 Summary



Due to the ultra short transmitted pulse, the receiver will resolve a ultra long delay spread channel. The average total received energy is distributed over a number of multipath arrivals. Although the equalizer mentioned in Section 3.3 can capture most multipath energy, this will induce high complexity. Furthermore, Rake diversity combining is another technique to effectively capture multipath energy. But the multipath induced ISI which will degrade system performance cannot be eliminated. Hence, a joint design of S-Pre-Rake scheme at transmitter and simple equalizer at receiver which can achieve both diversity combining and ISI elimination is proposed in this chapter. Computer simulations show that the proposed joint design systems have much lower complexity with insignificant performance degradation.

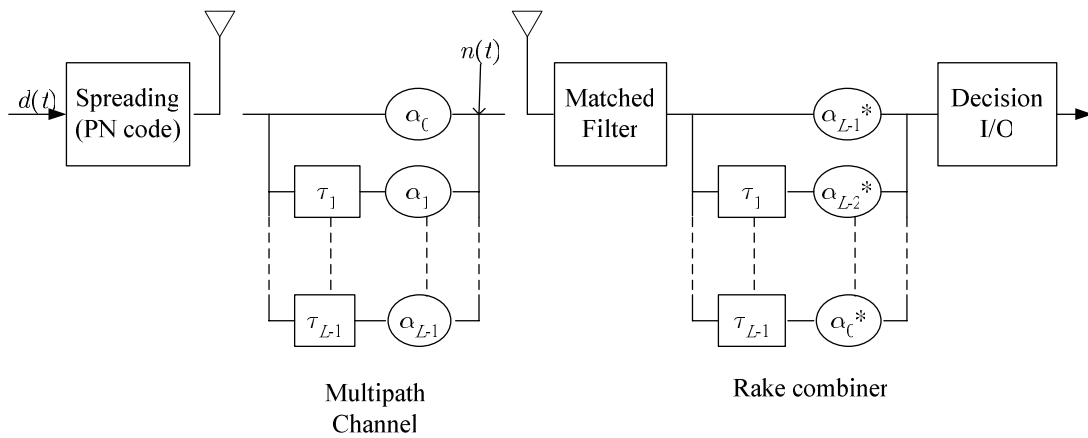


Figure 4.1 Block diagram of the Rake system

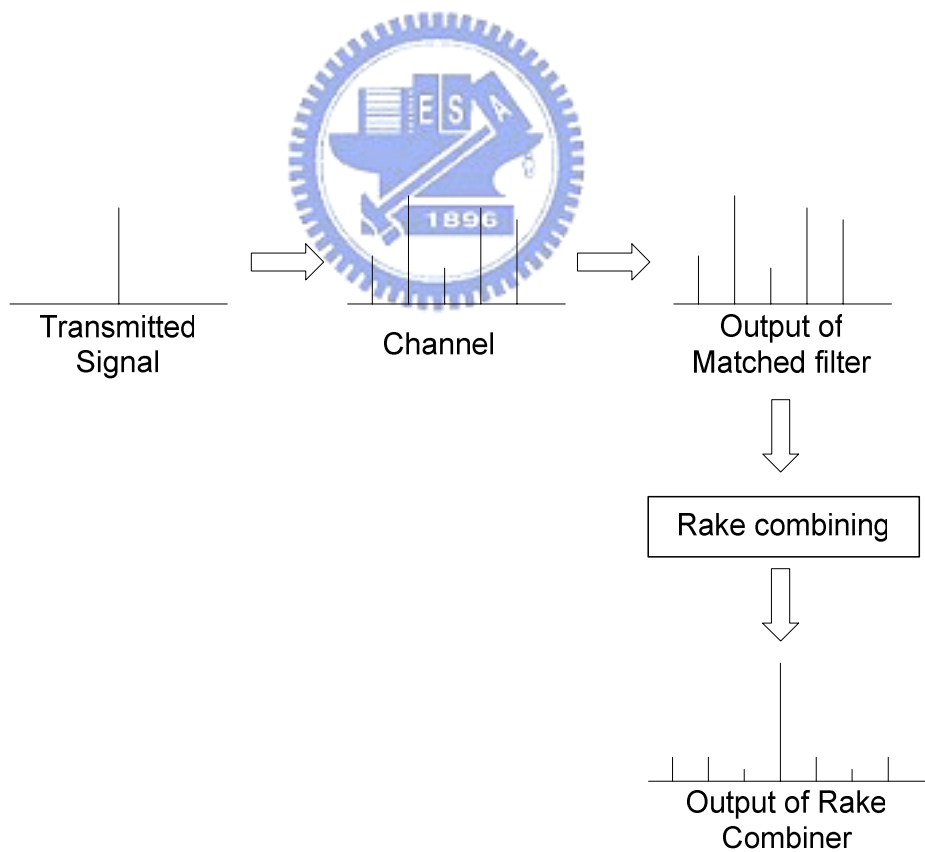


Figure 4.2 Rake combining concept

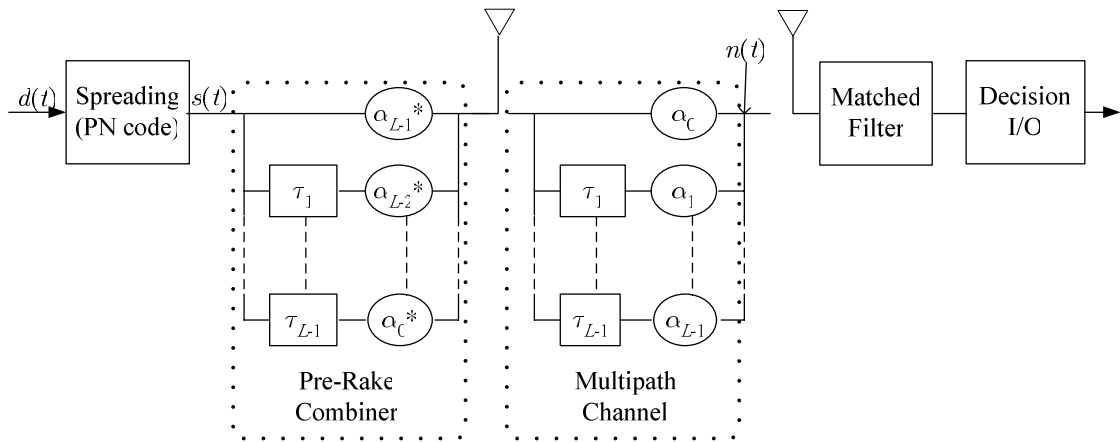


Figure 4.3 Block diagram of the Pre-Rake system

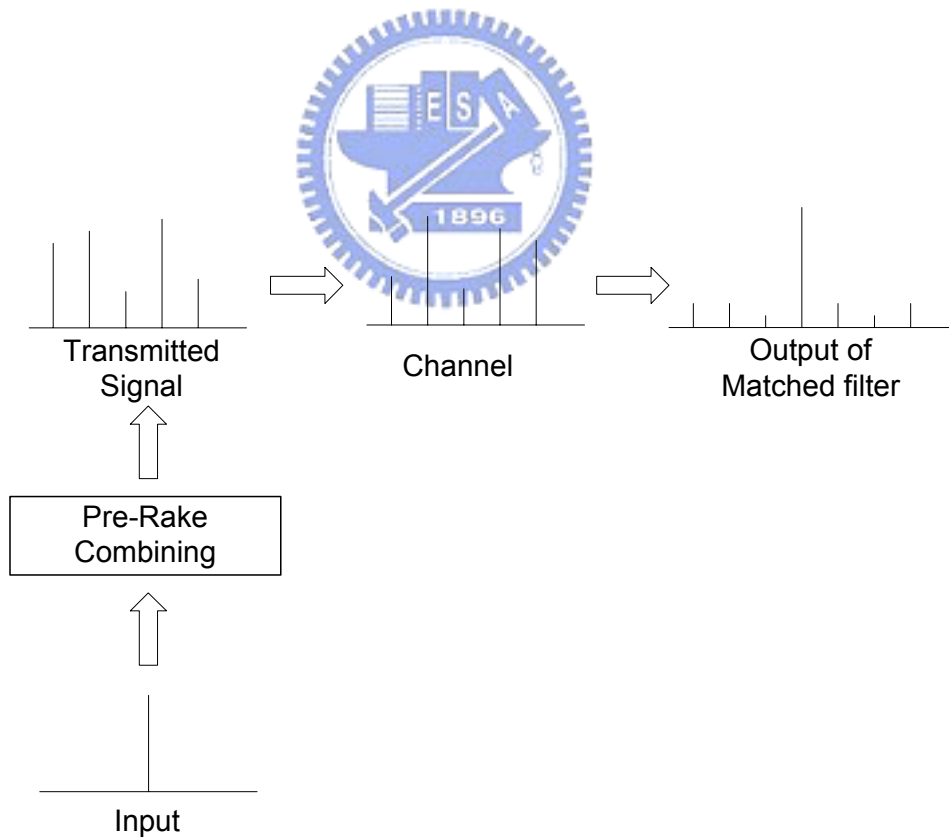


Figure 4.4 Pre-Rake combining concept

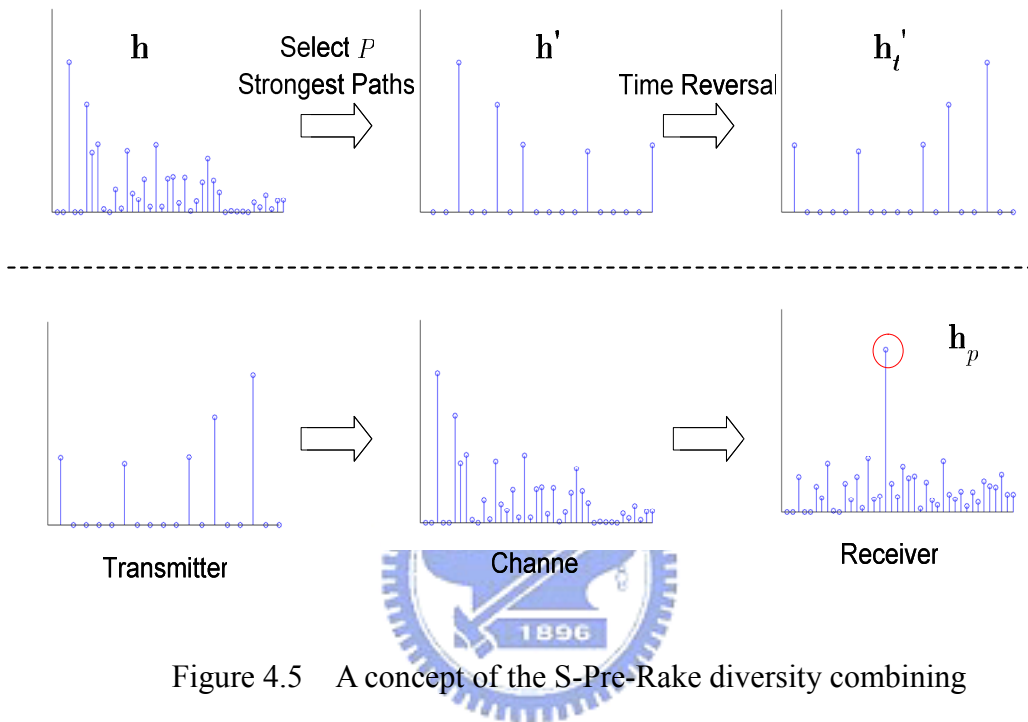


Figure 4.5 A concept of the S-Pre-Rake diversity combining

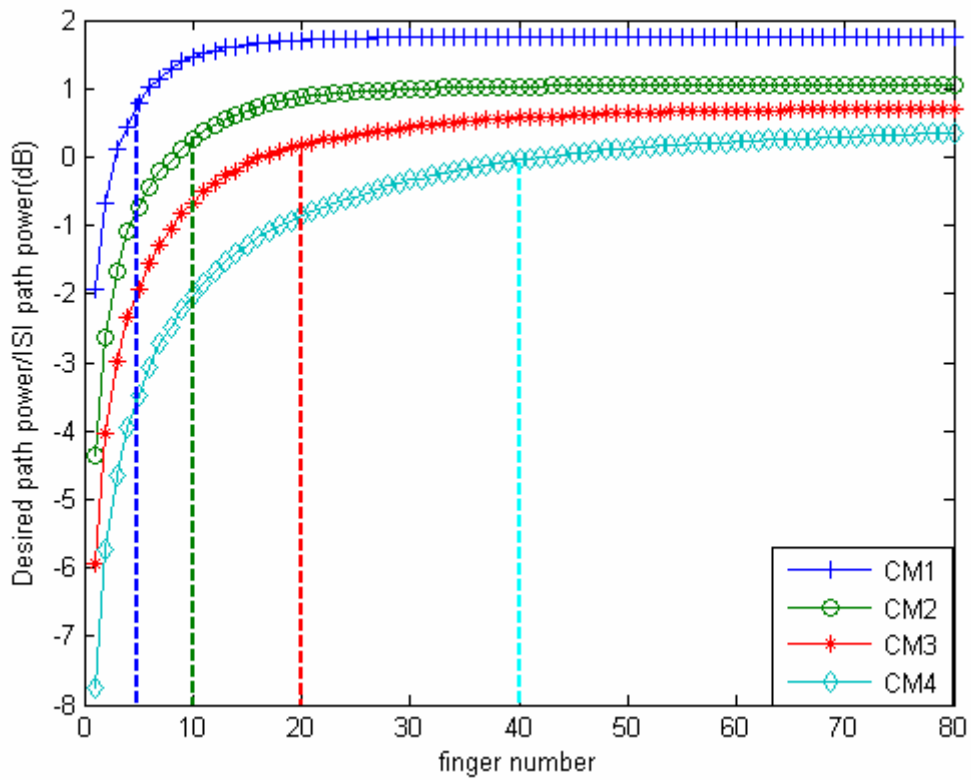


Figure 4.6 Ratio of desired path power to ISI path power P_D/P_{ISI} VS finger numbers

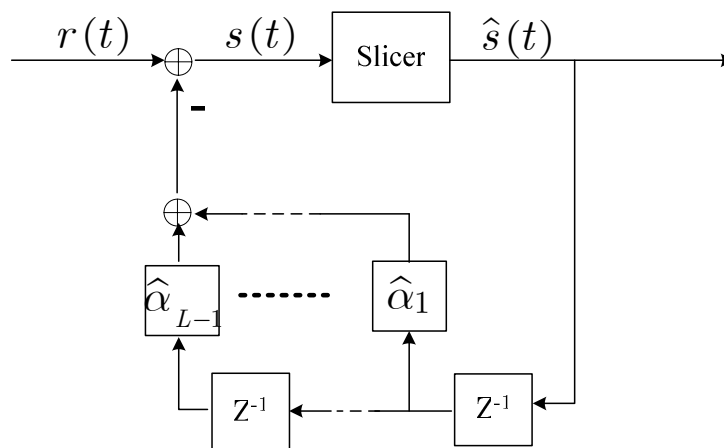
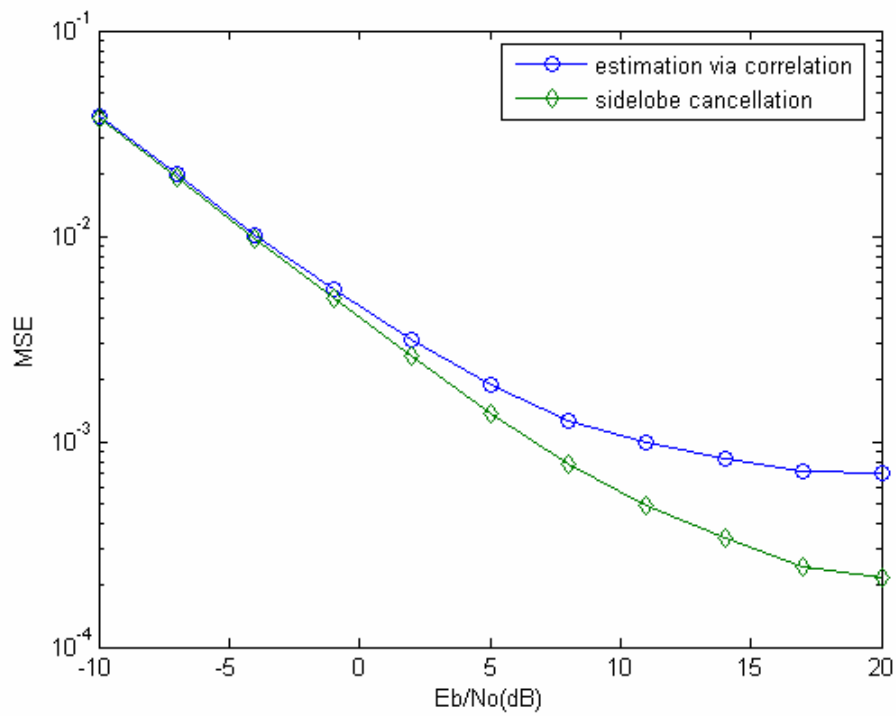
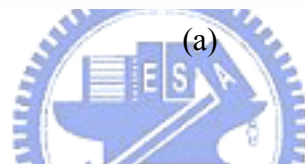
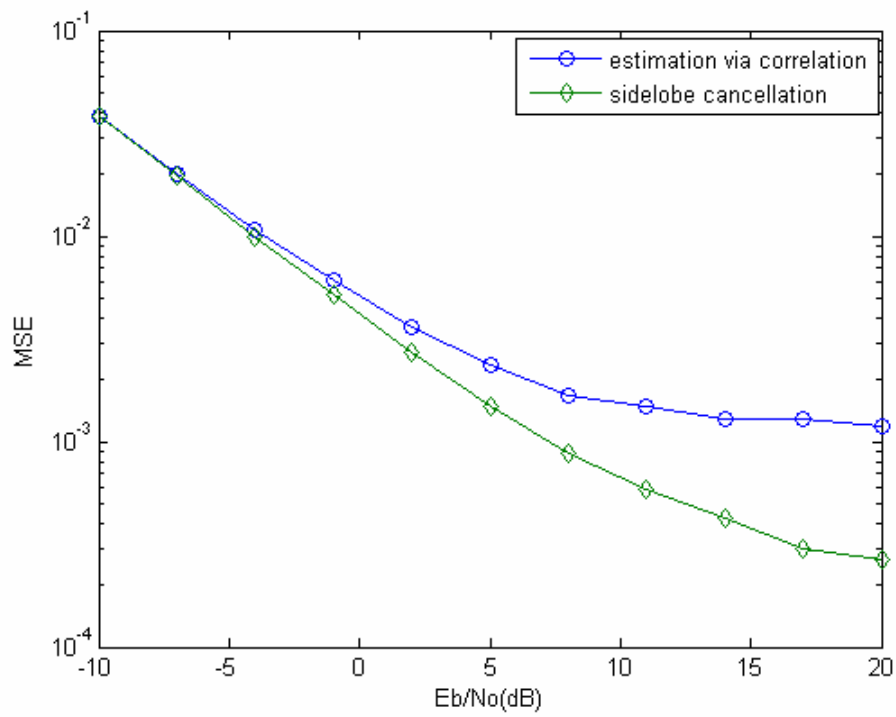


Figure 4.7 PCMC DFE structure



(b)

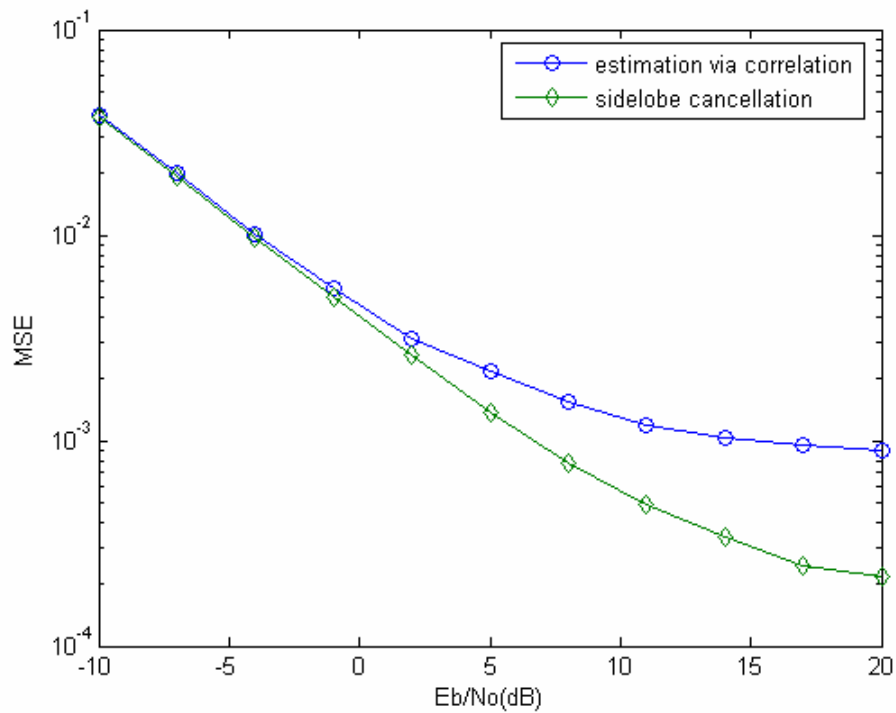
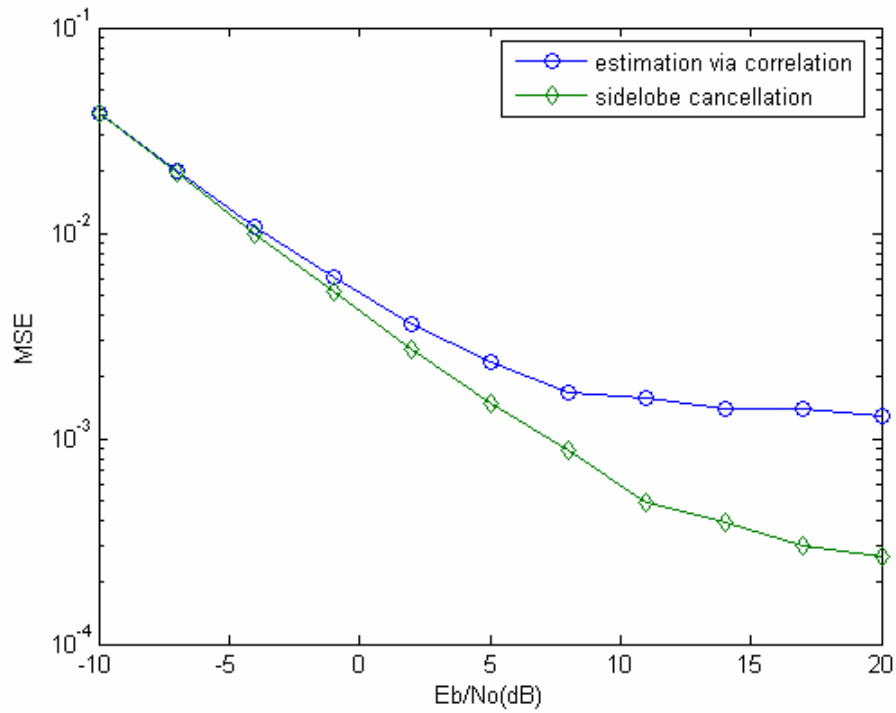


Figure 4.8 MSE of different channel estimation methods under different environments. (a) CM1 (b) CM2 (c) CM3 (d) CM4

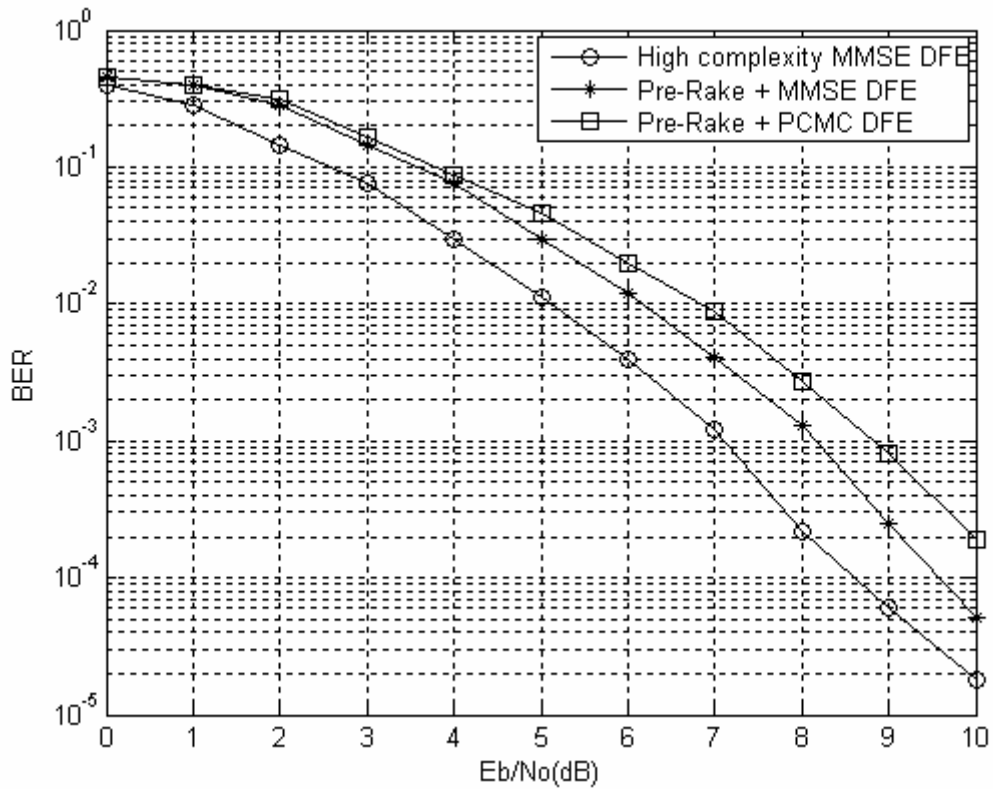


Figure 4.9 BER performances of the DS-UWB system of 110 Mbps data rate in CM3 by using S-Pre-Rake diversity combining and different equalizer types compared with high complexity equalizer

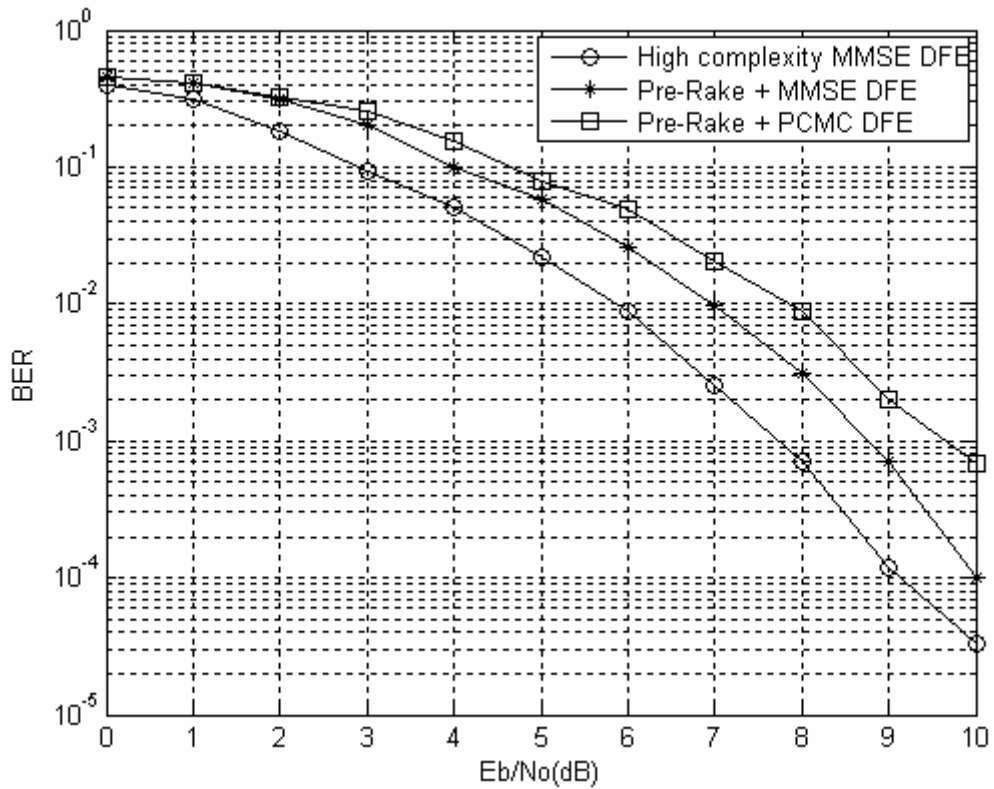


Figure 4.10 BER performances of DS-UWB system of 110 Mbps data rate in CM4 by using S-Pre-Rake diversity combining and different equalizer types compared with high complexity equalizer

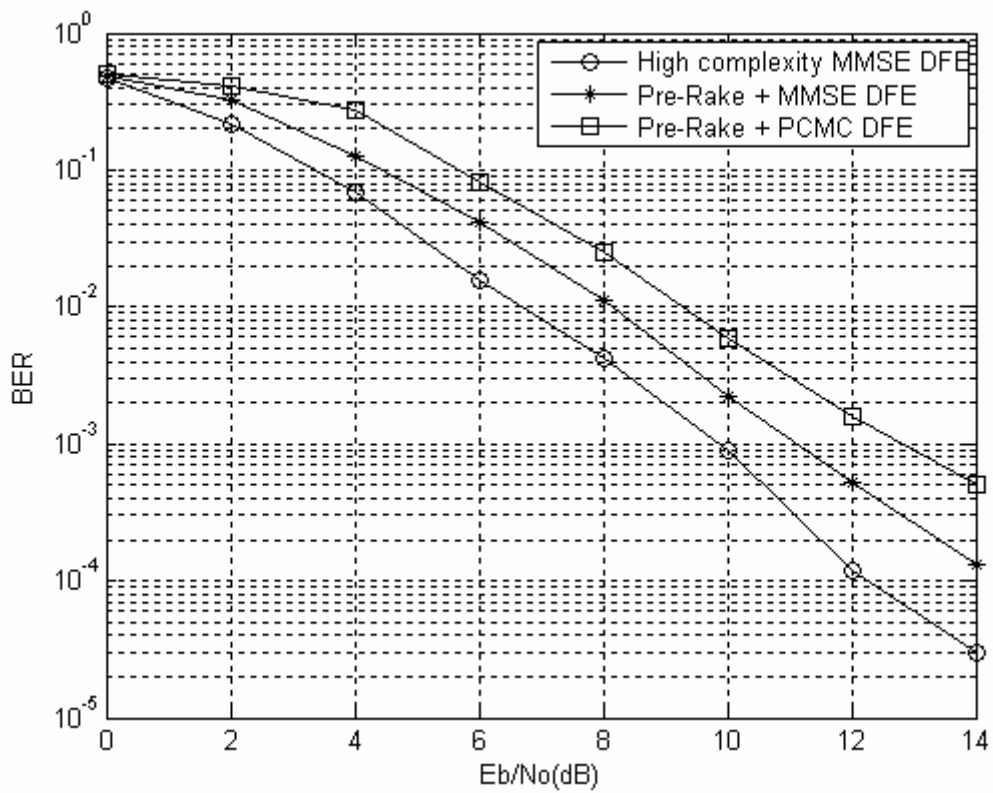


Figure 4.11 BER performances of DS-UWB system of 220 Mbps data rate in CM3 by using S-Pre-Rake diversity combining and different equalizer types compared with high complexity equalizer

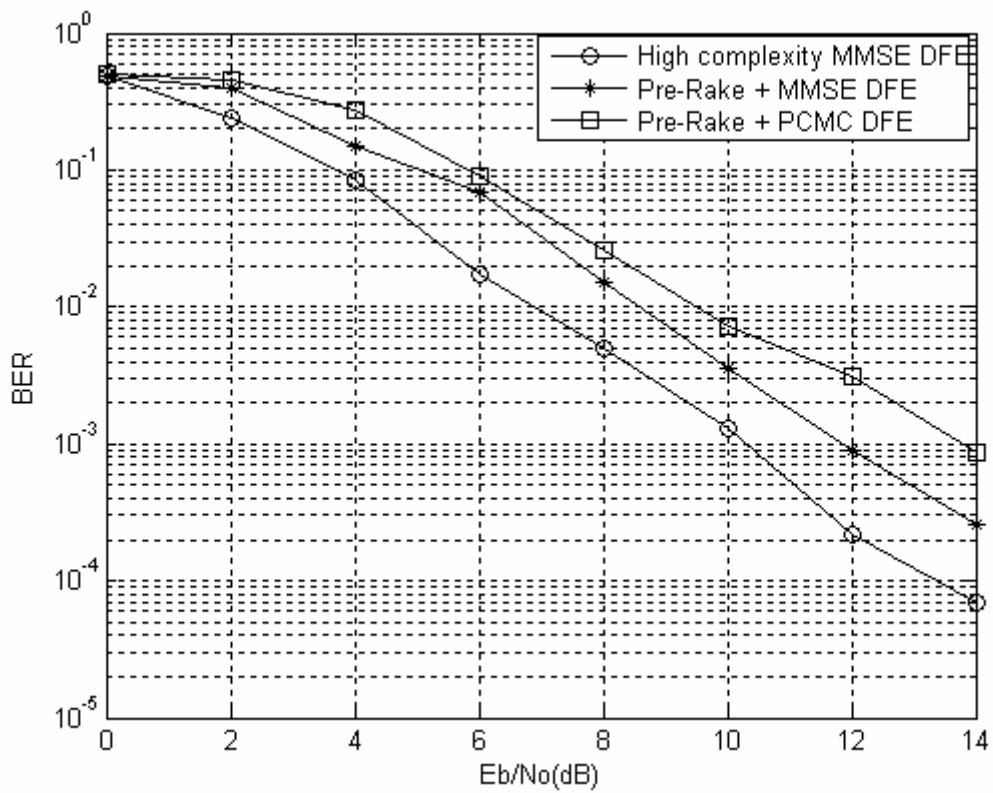


Figure 4.12 BER performances of DS-UWB system of 220 Mbps data rate in CM4 by using S-Pre-Rake diversity combining and different equalizer types compared with high complexity equalizer

Table 4.1 S-Pre-Rake finger numbers requirement for different environments

	CM 1	CM 2	CM 3	CM 4
S-Pre-Rake finger number	5	10	20	40

Table 4.2 Equalizer tap numbers of proposed joint design system for different environments

	CM3	CM4
MMSE DFE FFF	16	30
MMSE DFE FBF	16	30
PCMC DFE	16	30

Chapter 5

Conclusion

In this thesis, we propose an IEEE 802.15.3a DS-UWB system incorporating enhanced early-late (EL) code tracking loop and selective-Pre-Rake (S-Pre-Rake) diversity combining schemes. Compared to the conventional DS system, the receiver can resolve a dense and long delay spread channel impulse response due to the transmitted ultra short pulse.

In Chapter 2, concepts of DS system and specification of IEEE 802.15.3a DS-UWB system has been introduced. In Chapter 3, we first introduce the S-V model to form indoor UWB channel environment. Compared with usual narrowband channel model, the clustering phenomenon is the most notable characteristic in the channel. Next, we construct a simulation platform of an IEEE 802.15.3a DS-UWB system using Matlab. Synchronization and equalization algorithms for DS-UWB receiver are established. In particular, the dense and long delay spread multipaths will lead some receiver function blocks to be modified. The dense multipaths will cause the conventional EL code tracking loop to loose accuracy; the proposed EL code-tracking loop with multipath cancellation scheme can effectively overcome this problem. Besides, the channel length is different under different situations (CM1 to CM4), and we have defined different numbers of equalizer tap, respectively.

In Chapter 4, we introduce S-Pre-Rake diversity combining scheme to capture multipath energy without using a high complexity equalizer. Although the equalizer mentioned in Chapter 3 can capture most multipath energy, this will induce extreme high complexity. Furthermore, Rake diversity combining is another technique to effectively capture multipath energy. But the multipath induced ISI which will degrade system performance can not be eliminated. Hence, a joint design of S-Pre-Rake scheme at the transmitter and simple equalizer at the receiver which can achieve both diversity combining and ISI elimination simultaneously is proposed. Compared with the conventional equalizer, the proposed methods have much lower complexity with insignificant performance degradation.

The study presented in the thesis has thoroughly discussed the transceiver design for an IEEE 802.15.3a DS-UWB system and its efficacy has been rigorously verified using the simulation platform. In particular, we deliver feasible solutions to advanced DS-UWB systems. In practice, there are yet several other limitations remaining to be considered in implementing a DS-UWB system, such as memory usage, operating speed, and gate counts. For the sake of fast development and low cost, the development platform should adopt a programmable prototyping communication system including the existing functions presented in the thesis.

Although the low transmission power enables DS-UWB systems to coexist with conventional communication systems without interfering them, the existing communication devices will be considered as high power narrowband interference (NBI). Providing a NBI suppression scheme can make the DS-UWB system more flexible and reliable.

Other important challenges include efficient circuitry for UWB pulse generation, broadband antenna design and power-efficient transceivers establish other major

circuit implementation challenges. Controlling the response of very wideband transmit and receive antennas is a considerable challenge. The received pulse at the receive input after the RF stage which is the convolution of the generated baseband pulse shape and the antenna responses is not precisely known, even in the absence of multipath. Since many UWB applications are expected to support mobility, the net transceiver power budget is an important consideration. A key advantage of UWB designs is that the highly linear power amplifiers are not required since the UWB pulse generator need only produce a peak-to-peak voltage swing on the order of 100 mV to meet the FCC spectral mask requirements that can be achieved by a suitable UWB waveform. While the low power of UWB emissions indicates the potential of greater integration of baseband and RF circuits into CMOS, there still exist some significant challenges. A notable one is the specification of the analog-to-digital conversion (ADC) needed in any UWB transceiver; architectures that require sampling of the UWB signal at the pulse rate are infeasible for integration into a volume product with present-day state of the art due to the high cost and power consumption that would be incurred.

Besides the DS-UWB system, another specification named MB OFDM is also designed to match the IEEE 802.15.3a standard. Both DS-UWB and MB OFDM are focusing on having the IEEE 802.15 standards group adopt their UWB specification as a standard. It's unclear at this point which one of them will win. It's very possible that both will eventually become part of the same standard, similar to 802.11a and 802.11b/g is with wireless LAN (WLAN). Compared with the MB OFDM system, the DS-UWB transmitter is significantly less complex because it consists of a simple high chip rate pulse generator and modulator having very low peak requirements. There are no Fast Fourier Transform (FFT), no complex window multipliers, no digital-to-analog conversion (DAC), and no multiplicity of frequency generators or

fast hopping synthesizers. And the lower modulation order can decrease the sampling bits of ADC. Furthermore, the peak to average power ratio (PAPR) is still a problem for the MB OFDM system. However, the MB OFDM system has the advantage to capture multipath energy with the FFT. Moreover, MB OFDM enables the designer to adapt the system to avoid using some specific bands in order to comply with other regulations set forth by other countries. This would help to alleviate strong NBI generated in those used bands.



Bibliography

- [1] L. Yang and G. B. Giannakis, "Ultra-wideband communications: an idea whose time has come," *IEEE Signal Processing Mag.*, vol. 21, no. 6, pp. 26-54, Nov. 2004.
- [2] FCC First Report and Order: In the matter of Revision of Part 15 of the Commission's Rules Regarding Ultra-Wideband Transmission Systems, FCC 02-48, April 2002.
- [3] G. R. Aiello and G. D. Rogerson, "Ultra-wideband wireless systems," *IEEE Microwave Ma.*, vol. 4, no. 2, pp. 36-47, June 2003
- [4] IEEE 802.15WPAN High Rate Alternative PHY Task Group 3a (TG3a) [Online]. Available: <http://www.ieee802.org/15/pub/TG3a.html>
- [5] WLAN Medium Access Control (MAC) and Physical Layer (PHY) Specifications, ANSI/IEEE 802.11, 1999.
- [6] Local and Metropolitan Area Networks, IEEE 802.3, 2002.
- [7] Universal Serial Bus Specification, Revision 2.0, 2000.
- [8] Standard for a High-Performance Serial Bus, IEEE 1394, 1995.
- [9] R. Fisher et al., "DS-UWB Physical Layer Submission to 802.15 Task Group 3a," IEEE 802.15-04/0137r3, Motorola, Inc. et al., July 2004
- [10] R. Fisher et al., "DS-UWB Proposal Update for IEEE P802.15 Working Group for Wireless Personal Networks (WPANs)," IEEE 802.15-64/04140r7, Motorola, Inc. et al., July 2004.
- [11] R. Fisher et al., "Merger#2 Proposal Update for IEEE P802.15 Working Group for Wireless Personal Area Networks (WPANs)," IEEE 802.15-64/022r0, Motorola, Inc. et al., Jan. 2004
- [12] A. Batra et al., "Multi-band OFDM Physical Layer Proposal" IEEE

- 802.15-03/267r6, Texas Instruments et al., Sept. 2003.
- [13] A. Batra et al., “Multi-band OFDM Physical Layer Proposal” IEEE 802.15-03/141r4, Texas Instruments et al., May 2003.
- [14] A. Batra et al., “MultiBand OFDM Physical Layer Proposal for IEEE 802.15 Task Group 3a,” MBOA-SIG, Sept. 2004.
- [15] A. Batra et al., “Multi-band OFDM Physical Layer Proposal for IEEE 802.15 Task Group 3a,” Texas Instruments et al., Mar. 2004.
- [16] S. Haykin, *Communication Systems, 4th ed.*, NY: John Wiley and Sons, 2000.
- [17] B. Sklar, *Digital Communications, 2nd ed.*, NJ: Prentice-Hall, Upper Saddle River, NJ, 2001.
- [18] A. J. Viterbi, *DS-CDMA: Principles of Spread Spectrum Communications*, Reading, MA: Addison-Wesley, 1995.
- [19] R. E. Ziemer and W. H. Tranter, *Principles of Communications : Systems, Modulation, and Noise, 5th ed.*, NY: John Wiley and Sons, 2002.
- [20] IEEE 802.15.3 standard, “Wireless Medium Access Control (MAC) and Physical Layer (PHY) Specifications for High Rate Wireless Personal Area Networks (WPAN),” 2003 Edition.
- [21] IEEE 802.11-97/96, Naftali Chayat, Sep. 1997.
- [22] A. Saleh and R. Valenzuela, “A Statistical Model for Indoor Multipath Propagation,” *IEEE JSAC*, vol. 5, no. 2, pp. 128–137, Feb. 1987.
- [23] H. Hashemi, “Impulse Response Modeling of Indoor Radio Propagation Channels,” *IEEE JSAC*, vol. 11, no. 7, pp. 967–978, Sept. 1993.
- [24] J. Foerster, Ed., “Channel Modeling Sub-committee Report Final,” IEEE802.15-02/490, Dec. 2002.
- [25] M. K. Simon, “Noncoherent Pseudonoise Code tracking performance of spread spectrum receivers,” *IEEE Trans. Commu.*, vol.25, pp.327-345, March 1977.
- [26] G. Fock, J. Baltersee, P. Schulz, and H. Myer, “Channel tracking for Rake receivers in closely spaced multipath environments,” *IEEE JSAC*, vol. 9, issue 12, pp. 2420-2431, Dec. 2001.

- [27] F. D. Natali, "AFC tracking algorithms," *IEEE Trans. Commu.*, vol. 32, no. 8, pp. 935-974, Aug. 1984.
- [28] R. Esmailzadeh and M. Nakagawa, "Pre-Rake diversity combining for direct sequence spread spectrum mobile communications systems," *IEICE Trans. Commun.*, vol. E76-B, no. 8, pp. 1008-1015, Aug. 1993.
- [29] G. L. Turin, "Introduction to spread spectrum antimultipath techniques and their application to urban digital radio," *Proc. of the IEEE*, vol. 68, no. 3, March 1980
- [30] J. K. Han, M. W. Lee, and H. K. Park, "Principal ratio combining for Pre/Post-Rake diversity," *IEEE Comm. Letters*, vol. 6, no. 6, pp. 234-236, June 2002.
- [31] M. Jun and T. Oh, "Performance of Pre-Rake combining time hopping UWB system," *IEEE Trans. Consumer Electronics*, vol. 50, no. 4, pp. 1033-1037, Nov. 2004.
- [32] S. Imada and T. Ohtsuki, "Pre-Rake diversity combining for UWB systems in IEEE 802.15 UWB multipath channel," *Joint with Conference on Ultrawideband Systems and Technologies*, pp. 236-240, May 2004.
- [33] C. A. Montemayor and P.G. Flikkema, "Near-optimum iterative estimation of dispersive multipath channels," *IEEE Veh. Technol. Conference*, vol. 3, pp. 2246-2250, 1998.
- [34] P. Shan and E. J. King, "Cancel multipath interference in spread spectrum communications," *Wireless Systems Design Technology Report*, pp. 49-52, March 2001.

直接序列超寬頻系統於密集路徑通道下之同步與等化技術之研究



交通大學電機資訊學院
電信工程學系碩士班

鄭永立